Intranasal spike and nucleoprotein fusion protein-based vaccine provides cross-protection and reduced transmission against SARS-CoV-2 variants

Check for updates

Zineb Lakhrif[1], Agathe Poupée-Beaugé[1], Fanny Boursin [1], Céline Ducournau [1], Louis Lantier[1], Nathalie Moiré[1], Rodolphe Carpentier[2], Christelle Rossignol[3], Marianne Maquart[4], Fabienne Jospin[5,6], Laetitia Merat[7], Mireille Caul-Futy[8], Yazdan Yazdanpanah[9], Amel Bouakane[10], Mickael Riou[7], Antoine Touzé[11], Jean-François Eléouët[12], Charles-Adrien Richard [12], François Helle [13], Sophie Le Poder[14], Bernard Klonjkowski [14], Nicolas Meunier[14], Stéphan Zientara[14], Stéphane Paul [5], Marie-Noëlle Mévélec[1], Nicolas Aubrey[1,15], Mathieu Epardaud[1,15] ✉ & Isabelle Dimier-Poisson[1,15] ✉

The effectiveness of intramuscular vaccines aimed at preventing severe COVID-19 remains limited due to waning immunity and the emergence of novel variants. Next-generation vaccines are needed for broader protection and blocking virus transmission. Here, we rationally designed an original nasal subunit vaccine composed of a fusion protein (SwFN) made of Wuhan spike and nucleoprotein combined with biocompatible mucosal nanocarriers (Nc). In mouse model, the nasal Nc-SwFN vaccine elicited multivalent serum and mucosal neutralizing antibodies. Robust spike and nucleoprotein cross-reactive immunity against variants was induced with a predominant phenotype of resident memory T cells in the lungs. Moreover, Nc-SwFN led to protective responses against Wuhan and Delta infection in relevant models with an absence of morbidity, mortality, and virus dissemination in the lungs and brain. Finally, Nc-SwFN drastically reduced host-to-host transmission. These promising results underscore the advantages of the nasal Nc-SwFN approach as a broad-spectrum vaccine candidate against current and emerging SARS-CoV-2 variants.

SARS-CoV-2 has caused the most severe global health crisis in a century resulting in significant morbidity and mortality. In response to this emergency, numerous vaccines have been rapidly developed to target the original Wuhan strain with fourteen vaccines granted Emergency Use Listing by the WHO. Subsequently, three bivalent vaccines have been added to the vaccinal arsenal strategy to counter the rapid spread of SARS-CoV-2 variants, notably those from the Omicron line (WHO - Prequalification of Medical Products). Currently, all approved vaccines are administered intramuscularly and are based solely on the spike protein due to its high antigenicity and immunogenicity allowing the induction of a robust

¹BioMAP, UMR ISP1282 INRAe-Université, Tours, France. ²Univ. Lille, Inserm, CHU Lille, U1286 - INFINITE - Institute for Translational Research in Inflammation, Lille, France. ³INRAe, Université de Tours, ISP, Nouzilly, France. ⁴MAVIVH, INSERM U1259, Université de Tours, Tours, France. ⁵CIRI, Centre International de Recherche en Infectiologie, GIMAP team, Université de Lyon, Inserm, Université Claude Bernard, ENS Lyon, France. ⁶Immunology Laboratory, Reference Center 21 iBioThera, CHU Saint-Étienne, Saint-Étienne, France. ⁷INRAE, UE-1277 Plateforme d'Infectiologie Expérimentale (PFIE), Centre de Recherche Val de Loire, Nouzilly, France. ⁸Epithelix Sarl, 18 Chemin des Aulx, Plan-les-Ouates, Geneva, Switzerland. ⁹ANRS|Emerging Infectious Diseases/Inserm, Paris, France. Service de Maladies Infectieuses et Tropicales, Hôpital Bichat, AP-HP, Paris, France. ¹⁰ANRS|Emerging Infectious Diseases/Inserm, Paris, France. ¹¹Biologie des infections à Polyomavirus team, UMR ISP1282 INRAe-Université, Tours, France. ¹²Unité de Virologie et Immunologie Moléculaires, INRAe, Université Paris Saclay, Jouy en Josas, France. ¹³Agents infectieux résistance et chimiothérapie Research Unit, UR4294, Jules Verne University of Picardie, Amiens, France. ¹⁴UMR VIROLOGIE, INRAE, Ecole Nationale Vétérinaire d'Alfort, ANSES, Laboratoire de santé animale, Université Paris-Est, Maisons-Alfort, France. ¹⁵These authors contributed equally: Nicolas Aubrey, Mathieu Epardaud, Isabelle Dimier-Poisson. ✉e-mail: mathieu.epardaud@inrae.fr; isabelle.poisson@univ-tours.fr

systemic immune response, particularly the production of neutralizing antibodies. However, these vaccines, due to their parenteral administration, primarily prevent severe outcomes of COVID-19 and do not significantly impact infection rates and virus transmission[1]. Consequently, despite vaccination, the risk of generating new mutants remains high following infection[2,3]. The development of second-generation vaccines, able to induce mucosal immunity at the primary site of viral infection, is imperative to limit virus contagiousness and control the COVID-19 transmission and SARS-CoV-2 variation. Nasal vaccines offer an attractive alternative to injectable vaccines and offer promise for respiratory infectious diseases with unmet medical needs and potential future pandemics. They have the capacity to elicit both humoral and cellular-mediated immune responses at systemic and mucosal levels. Nasal vaccines can stimulate the production of neutralizing IgA antibodies in the respiratory tract and promote lung-resident T and B memory cells allowing long-term protection against viral replication and transmission[4–6]. Moreover, mucosal IgA exhibits multivalency and cross-protective activity across different SARS-CoV-2 variants[4,7,8].

Concurrently, considerable efforts have been directed towards developing mucoadhesive and biocompatible delivery systems to prolong nasal retention and enhance antigen uptake by antigen-presenting cells (APCs) in the respiratory tract[9,10]. Maltodextrin mucoadhesive nanocarriers (Nc) provide a suitable approach to stimulate mucosal and systemic immunity by improving the stability, absorption, and retention time of antigenic molecules in the nasal mucosa[9,10].

Furthermore, the emergence of SARS-CoV-2 variants able to escape spike antibody neutralization underscores the limitations of current spike-based vaccines. Given the necessity for multivalence in next-generation vaccines, we hypothesize that a vaccine targeting the nucleoprotein, a more conserved viral protein, in addition to the spike protein, would confer broader and long-lasting protection by eliciting cross-reactive cellular immunity against SARS-CoV-2 variants[11].

In this study, we have engineered a nasal subunit vaccine composed of an original heteromultimeric fusion protein consisting of 6 spike proteins and 2 nucleoproteins combined with biocompatible mucosal Ncs. Our findings demonstrate that Nc-SwFN eliciting a robust protective immunity characterized by (1) systemic and mucosal neutralizing antibodies targeting the spike protein, (2) spike and nucleoprotein-specific T-cell responses against SARS-CoV-2 variants, and (3) lung-resident memory T cells involved in the limiting the spread of SARS-CoV-2 spread.

Challenge studies conducted in mouse and hamster models have revealed that Nc-SwFN confers substantial protection against COVID-19 morbidity, mortality, virus dissemination in the lungs, nasal turbinates and brain. Notably, the Nc-SwFN vaccine not only prevents nasal virus shedding but also block virus transmission from vaccinated to unvaccinated animals.

Our findings suggest that the nasal Nc-SwFN vaccine approach may hold promise as a broad-spectrum vaccine candidate against current and emerging SARS-CoV-2 variants.

Results
SwFN protein was associated with the mucosal nanocarrier surface and could mimic the native virion morphological features
The vaccine SwFN fusion protein was designed with two different chains (Fig. 1A). The heavy chain (SwFN-hc) consists of the Wuhan ectodomain of the spike protein with a trimerization sequence, the hinge-CH2-CH3 assembly and then the nucleoprotein. Thus, the heavy chain will be dimerized *via* the hinge-CH2-CH3. In order to have a trimeric spike, a light chain (Sw-lc), consisting of the ectodomain of the spike protein and the trimerization sequence, was added. Several light chains can be self-assembled with the heavy chain dimer. Thereby, the fusion protein represented a heteromultimeric fusion protein, consisting of 6 spike proteins (2 trimer bouquets) and 2 nucleoproteins (Fig. 1A). Despite the considerable size of the SwFN protein (~1000 kDa), its production yield was in the order of 60 mg/L, and its purification was facilitated by the use of protein A affinity chromatography which allowed the recovery of only SwFN fusion protein (with SwFN-hc and Sw-lc) without soluble trimeric spike protein (Sw).

Purification of the non-retained supernatant proteins via the C-tag has allowed the isolation of a small amount of soluble Sw protein (Supplementary Fig. 1). These results proved the co-expression of SwFN-hc and Sw-lc chains and their association.

To evaluate the added value of nucleoprotein, a similar heteromultimeric protein control (SwF) was engineered (Fig. 1B) and produced at 75 mg/L. Spike of Wuhan (Sw), Delta (Sd), and Omicron (So) strains were also produced in trimeric form to study the induced spike-specific cell immune response against these variants.

Thermal profiles of the produced proteins were analyzed (Fig. 1C). The conformational changes were particularly visible in the first derivative. In comparison with Sw, the conformational changes due to the CH3 domain presented in SwF protein were observed at Tm 81.4 °C. The remaining profile was quite similar. The profiles of SwFN and SwF were particularly marked by the different conformational changes observed at 47.2 °C, which was obviously influenced by the presence of the nucleoprotein. These results confirmed the correct conformation of the SwFN fusion protein with its different parts.

Exclusion-diffusion chromatography analysis of SwF and SwFN proteins showed similar monomers and oligomers profile but with small shift in SwFN elution volume (Fig. 1D). This shift was certainly due to the increase in protein size with the nucleoprotein allowing faster protein elution.

The SwFN protein bind specifically with human anti-SARS-CoV-2 Spike Protein S1 Receptor-Binding Domain blocking antibody and rabbit anti-SARS-CoV-2 nucleoprotein antibody (2 commercial monoclonal antibodies) (Fig. 1E).

Proteins were complexed with mucosal Ncs with a ratio of 3:1 (Nanocarriers: Protein). Analysis of the vaccine preparation by Native Page with silver nitrate sensitive staining did not reveal free proteins confirming total protein association to Ncs (Fig. 1F).

Protein complexation with Ncs was visualized with transmission electronic microscopy (TEM) (Fig. 1G). Part of the SwFN protein appears to be associated with the nanocarrier surface, probably through electrostatic interactions. The protein vaccine interaction with the human nasal mucosa was studied using MucilAir™ cell model. At short-time (30 minutes), Nc-SwFN was observed in contact with the vibrating cilia of epithelial cells (Fig. 1H). The vaccine protein was protected by the mucus and was internalized mainly by mucus cells after 6 hours, in specific vesicles (Fig. 1I). Nc-SwFN did not cause any physiological changes in the mucosal tissue.

Complexation of the vaccine protein with mucosal Ncs was a prerequisite to induce humoral immunogenicity at mucosal level
The analysis of humoral immunogenicity, especially in mucosal compartments, is a key feature to confirm the importance of using Ncs as a nasal vaccine delivery system. To prove the added value of maltodextrin mucosal Ncs, female Balb/c mice were immunized twice at three weeks of intervals by the intranasal route with the Nc alone, the SwFN soluble fusion protein (SwFN) or the SwFN complexed protein with the nanocarriers (Nc-SwFN). Humoral immune response was studied 7 days after the last immunization against the spike from the Wuhan variant and nucleoprotein by analyzing IgG and IgA antibodies in serum, nasal, and bronchoalveolar secretions. Only anti-spike antibodies were detected. Compared to the Nc control mice group, Nc-SwFN immunized mice produced significantly higher amounts of serum anti-spike IgG and IgA antibodies. Vaccination with SwFN soluble protein induced only the production of anti-spike IgG antibodies in serum but at a lower level (Fig. 2A, B). The ability of these antibodies to neutralize SARS-CoV-2 virus has been studied. Polymerase chain reaction-based live virus neutralization assays were used to quantify the titer of neutralizing antibodies in serum. For Wuhan strain, a pool of serum per group was used, and total neutralization can be observed until 1/80 serum dilutions for the Nc-SwFN group, whereas only 35% of virus neutralization was observed at 1/20 serum dilution for the SwFN immunized group with an NT50 for a 1/151 serum dilution (Fig. 2C). Delta strain neutralization was also studied with individual serum. Results showed a mean of 64% of virus neutralization

Fig. 1 | Characterizations of SwFN protein and Nc-SwFN vaccine. A Schematic representation of the heteromultimeric fusion protein. The two polypeptide chains constituting the fusion protein were presented at the far left, followed by the self-assembly thanks to the dimerization domain/ trimerization sequence block of the different chains. A schematic presentation of the isolated protein was mentioned on the right. **B** Schematic representation of the SwF heteromultimeric fusion protein without nucleoprotein. **C** Thermal analysis of the three proteins Sw, SwF, and SwFN. **D** exclusion-diffusion chromatography analysis of the SwF and SwFN fusion protein. **E** Sandwich ELISA shows the detection of the SwFN fusion protein by anti-N antibody after protein binding to the anti-S antibody. **F** Electrophoresis native PAGE of the SwFN fusion protein and vaccine complexations (Nc-SwF and Nc-SwFN). **G** Transmission electronic microscopy analysis of the SwFN (left), nanocarriers alone (medium), and the SwFN complexation with the nanocarriers (right). Arrowheads show examples of fusion proteins associated with the surface of the nanocarriers. Scale bar is 200 nm. **H** Vaccine uptake and **I** Internalization by the human nasal mucosa.
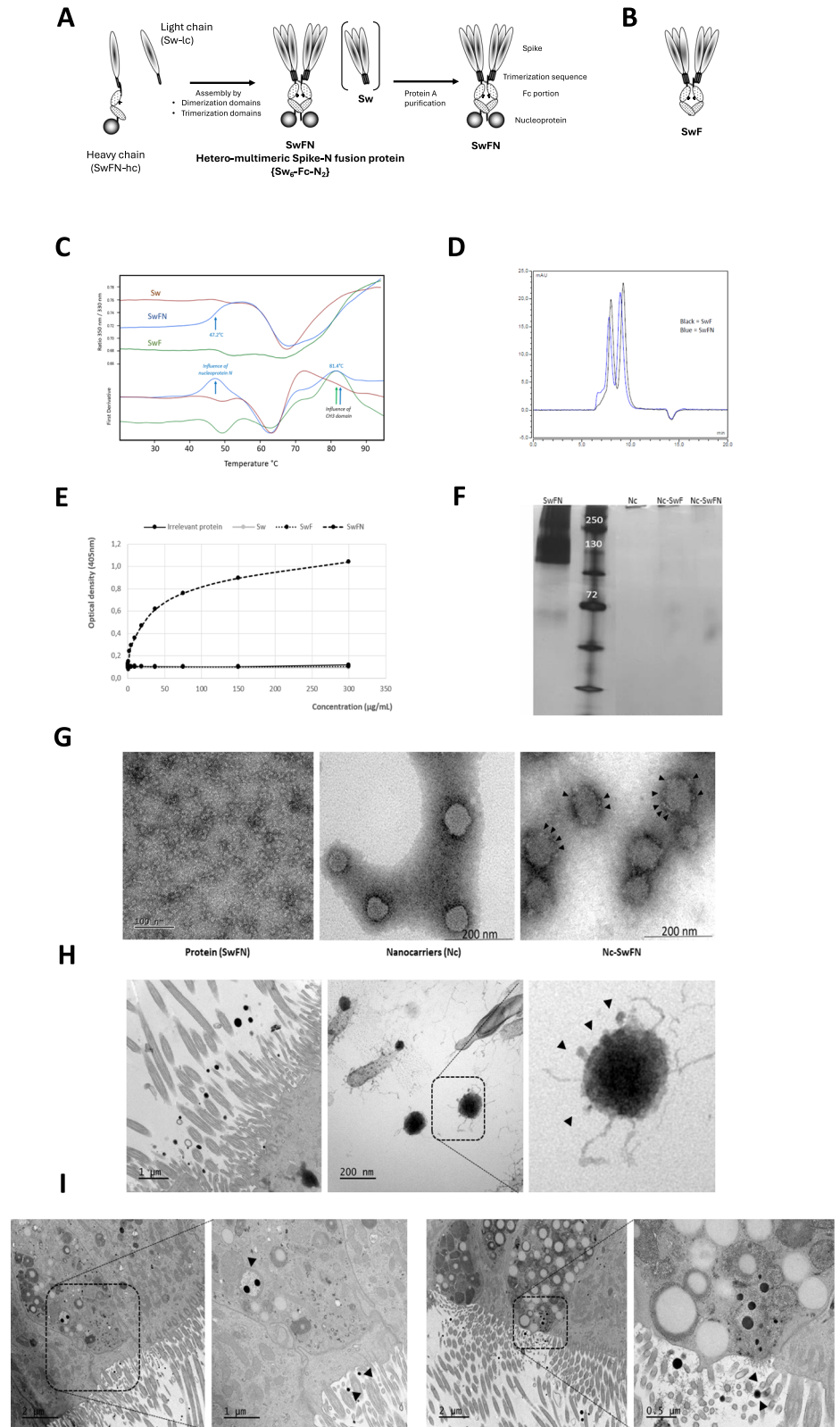
at 1/20 serum dilutions for the Nc-SwFN immunized group, with an NT50 for a 1/32 serum dilution, whereas SwFN group serum failed to produce neutralizing antibodies (Fig. 2D).

Further, humoral immune response analysis in mucosal compartments showed anti-spike antibody IgA production mainly in nasal and bronchoalveolar washes from Nc-SwFN immunized mice (Fig. 2E, F).

The percentage of mucosal antibody neutralization in nasal washes and bronchoalveolar lavages (BAL) was assessed only at a 1/5 dilution due to the limited sample volumes available, which restricted further dilution series for analysis.

In nasal washes samples, low (20–40%) to intermediate (40–60%) neutralization levels were detected in the Nc-SwFN immunized group
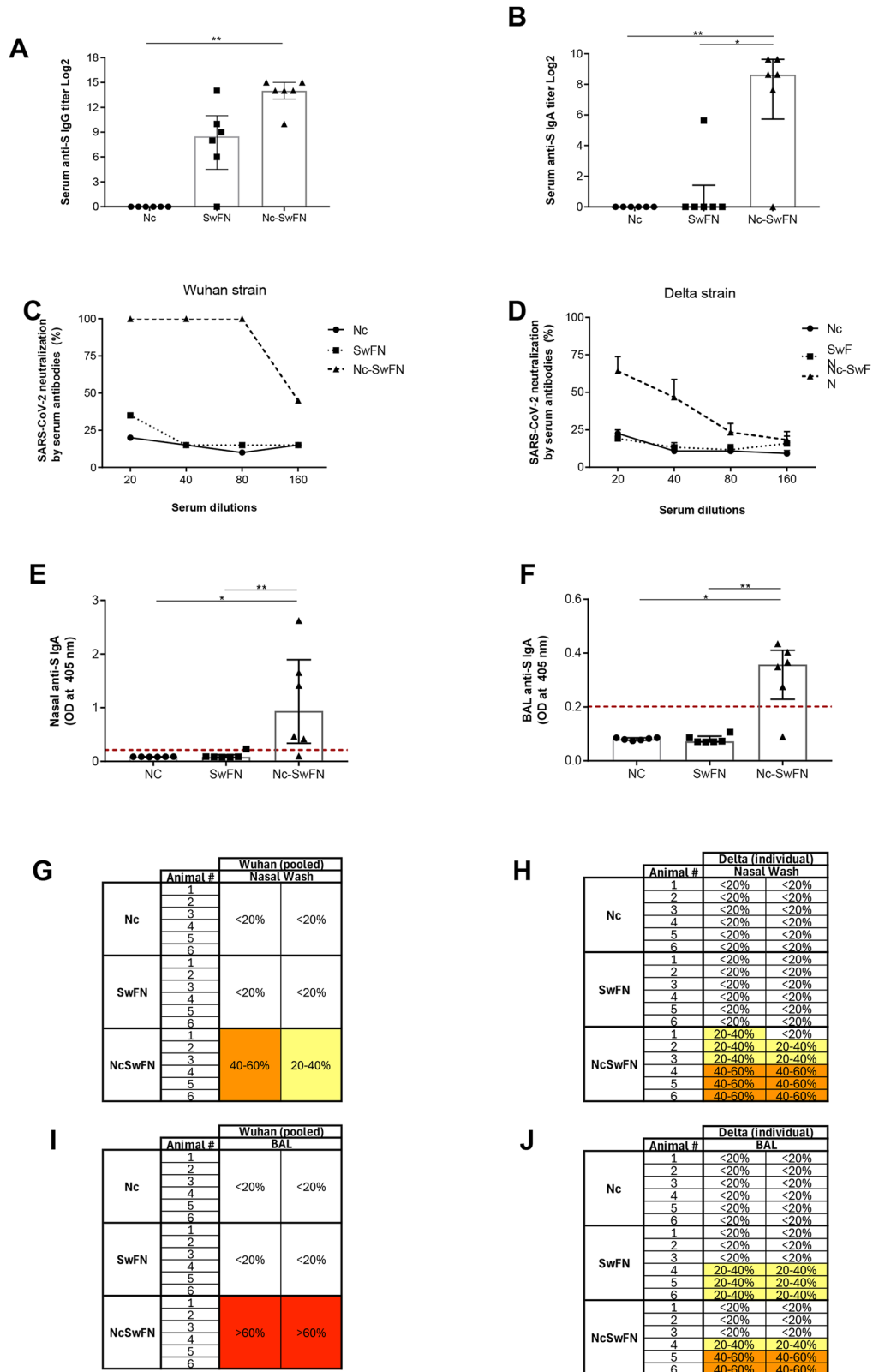
Fig. 2 | Humoral immune response against spike protein after SwFN and Nc-SwFN immunizations. Female Balb/c mice were immunized twice at 3-week interval by intranasal route with nanocarriers alone (Nc) ($n = 6$ animals), SwFN ($n = 6$ animals), and Nc-SwFN complexation ($n = 6$ animals). Serum IgG and IgA antibodies were analyzed by specific anti-spike ELISA 7 days after the last immunization and presented respectively in (**A**, **B**). Their neutralization capacity was tested against Wuhan (analysis of serum pool) (**C**) and Delta (analysis of individual serum from 6 immunized mice) strains (**D**). Nasal and BAL anti-spike IgA antibodies were analyzed by specific anti-spike ELISA 7 days after the last immunization and presented respectively in (**E**, **F**). The neutralization capacity of the mucosal sample was tested against Wuhan (analysis of mucosal samples pooled from the 6 animals) (**G**, **I**) and Delta (analysis of mucosal samples individual) (**H**, **J**) strains, at the 1/5 dilution (column are experimental duplicates); nasal samples (**G**, **H**) and bronchoalveolar lavage samples (**I**, **J**). Data were analyzed by two-way ANOVA and Kruskal–Wallis tests (*$p < 0.05$, **$p < 0.01$, ****$p < 0.0001$).

against both the Wuhan and Delta strains, while no neutralization was observed in samples from Nc or SwFN immunized groups (Fig. 2G, H).

In BAL samples, high levels of neutralization (>60%) were observed in samples of Nc-SwFN immunized group against the Wuhan strain with no detectable neutralization in the Nc and SwFN groups (Fig. 2I). Against the Delta strain, low (20–40%) to intermediate (40–60%) neutralization levels were detected in BAL samples from the Nc-SwFN group with undetectable or low neutralization in samples from Nc and SwFN groups (Fig. 2J).

These results confirmed the potency of vaccine protein complexation with mucosal Ncs to induce anti-spike neutralizing serum and mucosal antibodies.

Nc-SwFN vaccine potentiated the level of mucosal anti-spike antibodies regarding to spike-based vaccine

To confirm that the addition of nucleoprotein at the SwFN C-terminal end did not impact spike protein immune response outcome, the immunogenicity of SwFN vaccine complexation was compared to that of SwF complexation. Balb/c mice were immunized according to the same vaccination protocol, and the humoral immune response was analyzed 7 days after the last immunization against the Wuhan strain. Nc-SwF and Nc-SwFN immunized mice produced similar amounts of anti-spike serum IgG (Fig. 3A), but not serum IgA which seems to remain higher in Nc-SwFN immunized mice (Fig. 3B). As shown in Fig. 3C, D, Nc-SwF serum can only neutralize the Wuhan strain at low titer (1/20) while serum antibodies from Nc-SwFN mice, maintained Wuhan and Delta strain neutralization until 1/80 and 1/40, respectively.

Anti-spike IgA production was significantly higher in both nasal and bronchoalveolar washes of Nc-SwFN immunized mice compared to Nc-SwF immunized mice (Fig. 3E, F).

In nasal wash samples, low (20–40%) to intermediate (40–60%) neutralization levels were detected in both Nc-SwF and Nc-SwFN immunized groups against the Wuhan strain (Fig. 3G). Against the Delta strain, low (20–40%) neutralization was observed in the Nc-SwF immunized group, while low (20–40%) to intermediate (40–60%) neutralization levels were detected in the Nc-SwFN immunized group (Fig. 3 H). No neutralization was observed in nasal washes from Nc immunized group (Fig. 3G, H).

In BAL samples, low (20–40%) to intermediate (40–60%) neutralization levels were detected in the Nc-SwFN immunized group against both the Wuhan and the Delta strains, with undetectable neutralization in samples from Nc or Nc-SwF immunized groups (Fig. 3I, J).

To conclude, nucleoprotein position in SwFN vaccine design did not affect the production of serum anti-spike antibodies. More interestingly, its presence was even able to enhance the mucosal anti-spike antibody productions in nasal and bronchoalveolar levels probably through the induction of IgA-associated cytokines such as IL-2, IL-4, IL-5, and IL-10[12].

Nc-SwFN vaccine induced a specific cellular immune response against SARS-CoV-2 variants

To further investigate the immune efficacy of the fusion protein as a vaccine candidate against different variants of SARS-CoV-2, we explored the cellular immune response induced after Nc-SwFN immunization against nucleoprotein and spike protein from different variants. Systemic immune response was first evaluated against Wuhan spike protein by measurement of cytokine releases in stimulated-cell culture supernatant. As shown in Fig. 4A, IFN-γ production was comparable in Nc-SwF and Nc-SwFN immunized mice. The production of IL-2 and IL-17A cytokines was more prominent with higher levels in Nc-SwFN immunized mice, compared to Nc-SwF group (Fig. 4B, C).

Systemic immune response was then evaluated against Delta and Omicron spike proteins. No difference was observed in IFN-γ production between Nc-SwF and Nc-SwFN immunized mice (Fig. 4D, G). IL-2 production depended on the spike strain protein used, and surprisingly higher IL-2 level was detected after Nc-SwF spleen cell re-stimulation with Delta spike protein (Fig. 4E). Conversely, the IL-2 systemic production was higher

in Nc-SwFN immunized mice for Omicron spike-restimulated splenocytes (Fig. 4H). IL-17A production was higher in Nc-SwFN immunized mice whatever the spike protein used for spleen cell re-stimulation (Fig. 4F, I).

Moreover, only Nc-SwFN vaccination induced a nucleoprotein-specific cellular immune response with IFN-γ, IL-2, and IL-17A cytokine production (Fig. 4J–L).

The lung cellular immune response was also analyzed after Wuhan spike and nucleoprotein re-stimulations. RegardingAs compared to the Nc-SwF group, IFN-γ, IL-2, and IL-17A cytokine productions were more pronounced in Nc-SwFN immunized mice (Fig. 4M–R).

These results demonstrated the added value of Nc-SwFN vaccine compared to Nc-Sw spike-based vaccine. Nc-SwFN vaccination was able not only to produce anti-spike neutralizing antibodies at systemic and mucosal levels but also to induce specific cellular immune response against nucleoprotein, Wuhan, Delta and Omicron spike proteins, confirming the ability of this vaccine candidate to induce a protective immunity against SARS-CoV-2 variants.

Functional signatures of effector and memory T CD8+ and T CD4+ cells in spleens and lungs after Nc-SwFN vaccination

To evaluate the long-term effectiveness of Nc-SwFN vaccine, it was important to determine which T-cell subsets mediated the protective immunity, delineating their effector and memory functions. Cellular immune response was further analyzed in spleens and lungs one week after the last dose of Nc-SwFN vaccine compared to naive mice. Mice were injected intravenously with anti-CD45-BV510 to distinguish circulatory and tissue-resident T cells. The differences between parent cell percentage of these two groups are presented in table S1. Analysis of effector T cells in spleens showed a polyfunctional role of circulating CD45+ CD8+ T cells indicated by the simultaneous expression of IFN-γ, IL-2, TNF-α, and degranulation marker CD107A. Circulating CD45+ CD4+ T cells expressed degranulation marker CD107A eliciting cytotoxic function (Fig. 5A). In parallel, IFN-γ and CD107A expression was pronounced by both resident CD45− CD4+ and CD45− CD8+ T cells.

Intracellular cytokine staining in Nc-SwFN lungs highlighted the cytotoxic function of CD45+ CD8+ T cells and the IFN-γ mediated CD45+ CD4+ T cell effector function. For resident T cells in lungs, IFN-γ expression and cytotoxic function were mainly induced by CD45− CD8+ T cells. These cells additionally produced higher levels of TNF-α cytokine (Fig. 5B).

As shown in Fig. 5C, the most prominent T memory cells in spleens of Nc-SwFN-immunized mice were CD4+ T Central Memory cells (TCM: CD45+ KLRG1− CD127+ CD69− CD103−) followed by CD8+ T Effector Memory cells (TEM: CD45+ KLRG1+ CD127+) respectively. CD8+ T Resident Memory cells (TRM) were detected in the spleens with CD69− CD103+ predominant phenotype.

In lungs, only TCM cells were detected with an increase of T CD8+ CD45+ KLRG1− CD127+ CD69− CD103− cells. Similar to spleens, T CD8+ CD69− CD103+ resident memory cells were also detected in the lungs but the vast majority of induced TRM cells were CD4+ CD69+ CD103+ (Fig. 5D).

Beside the induction of circulating effector memory cells in spleens, both lung-resident and circulating memory T CD4+ and CD8+ cells were efficiently established. Inducing circulating and resident T cells should be more effective against breakthrough infections. Thereby, Nc-SwFN vaccine would be able to provide long-term protective immunity against SARS-CoV-2 virus.

Nc-SwFN vaccine protects K18-hACE2 mice from morbidity and mortality following infection with Delta SARS-CoV-2 variant

Following the encouraging Nc-SwFN immunogenicity results, we evaluated whether the induced protective immunity preserved mice from clinical symptoms and mortality of SARS-CoV-2 infection. Since the SwFN was designed with the Wuhan spike protein, vaccine protective effectiveness was evaluated against Delta SARS-CoV-2 variant, to highlight the added value of the nucleoprotein. Female human-ACE2 transgenic mice (K18-hACE2)

Fig. 3 | Spike specific humoral immune response induced after Nc-SwF and Nc-SwFN immunizations. Female Balb/c mice were immunized twice at 3-week interval by intranasal route with nano-carriers alone (Nc) ($n = 6$ animals), Nc-SwF ($n = 6$ animals) and Nc-SwFN complexation ($n = 6$ animals). IgG and IgA antibodies were analyzed by specific anti-spike ELISA 7 days after the last immunization. Serum anti-spike IgG and IgA were presented respectively in **A**, **B** with their neutralization capacity against Wuhan (**C**) and Delta strains (**D**). Nasal anti-spike IgA antibodies were showed in (**E**). BAL anti-spike IgA antibodies were showed in (**F**). The neutralization capacity of mucosal sample was tested against Wuhan (**G**, **I**) and Delta (**H**, **J**) strains, at the 1/5 dilution (column are experimental duplicates); nasal samples (**G**, **H**) and bronchoalveolar lavage samples (**I**, **J**). Data were analyzed by Kruskal–Wallis and one-way ANOVA tests (*$p < 0.05$, **$p < 0.01$, ***$p < 0.001$).
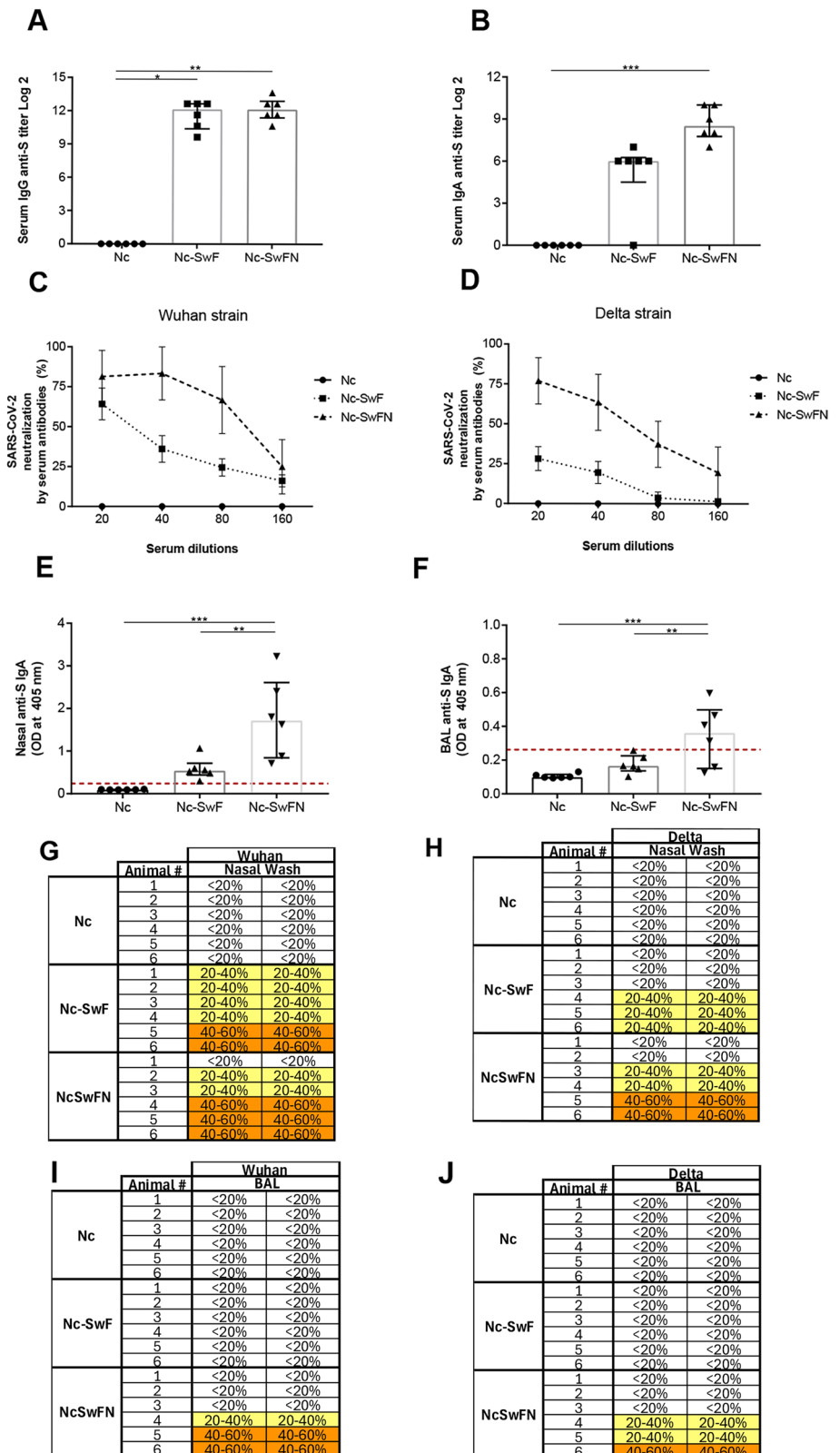
were immunized twice at three-week intervals by intranasal inoculation, with the mucosal Ncs alone, the Nc-SwF, or the Nc-SwFN fusion protein complexations. First, to focus on the appearance of clinical signs, mice were infected one week after the second immunization with 1.3×10^5 Tissue Culture Infective Dose 50% ($TCID_{50}$), sublethal dose, of Delta variant (Fig. 6A top). Eight days after infection, Nc control mice had extreme weight

loss, corresponding to more than 15% of their weight (cutoff point was 20%) (Fig. 6B). Mice immunized with Nc-SwF had lost an average of almost 10% of their weight. After Nc-SwFN immunization, body weight loss remained negligible, followed by weight gain after 6 days post-infection (p.i.), demonstrating vaccine effectiveness. Moreover, all Nc mice showed a decrease or even absence of activity. Third Nc-SwFN or Nc-SwF immunized
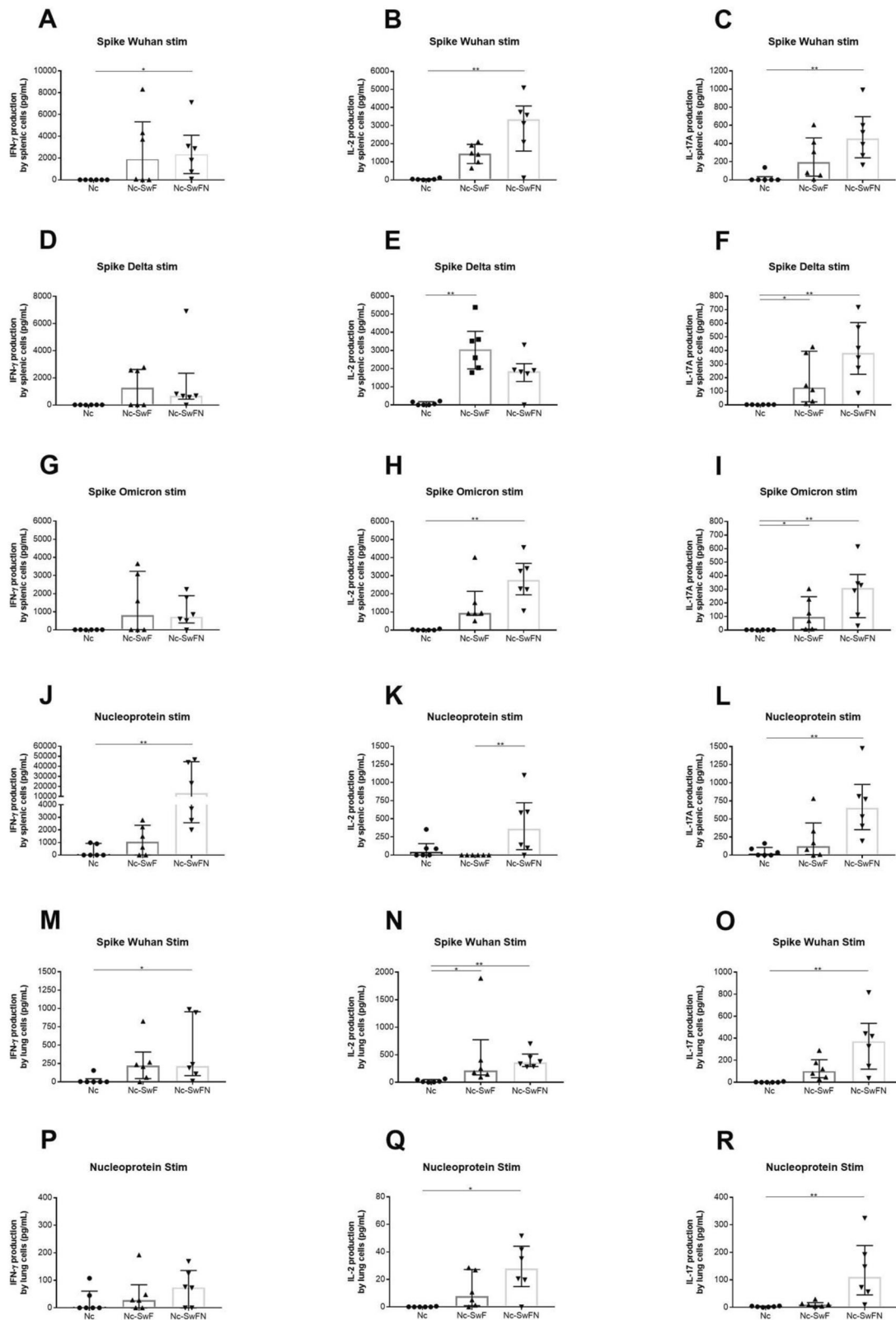
Fig. 4 | Systemic cellular immune response against nucleoprotein and spike SARS-CoV-2 variants after Nc-SwF and Nc-SwFN immunizations. Female Balb/c mice were immunized twice at 3-week intervals by intranasal route with nano-carriers alone (Nc) ($n = 6$ animals), Nc-SwF ($n = 6$ animals) and Nc-SwFN complexation ($n = 6$ animals). Spleen and lung cells were stimulated by nucleoprotein and spike protein from SARS-CoV-2 Wuhan, Delta, and Omicron strains and IFN-γ (**A**, **D**, **G**, **J**, **M**, and **P**), IL-2 (**B**, **E**, **H**, **K**, **N**, and **Q**) and IL-17 (**C**, **F**, **I**, **L**, **O**, and **R**) cytokines were quantified by MACSPlex Cytokine kit after 72 hours. Data were analyzed by Kruskal–Wallis test (*$p < 0.05$, **$p < 0.01$).
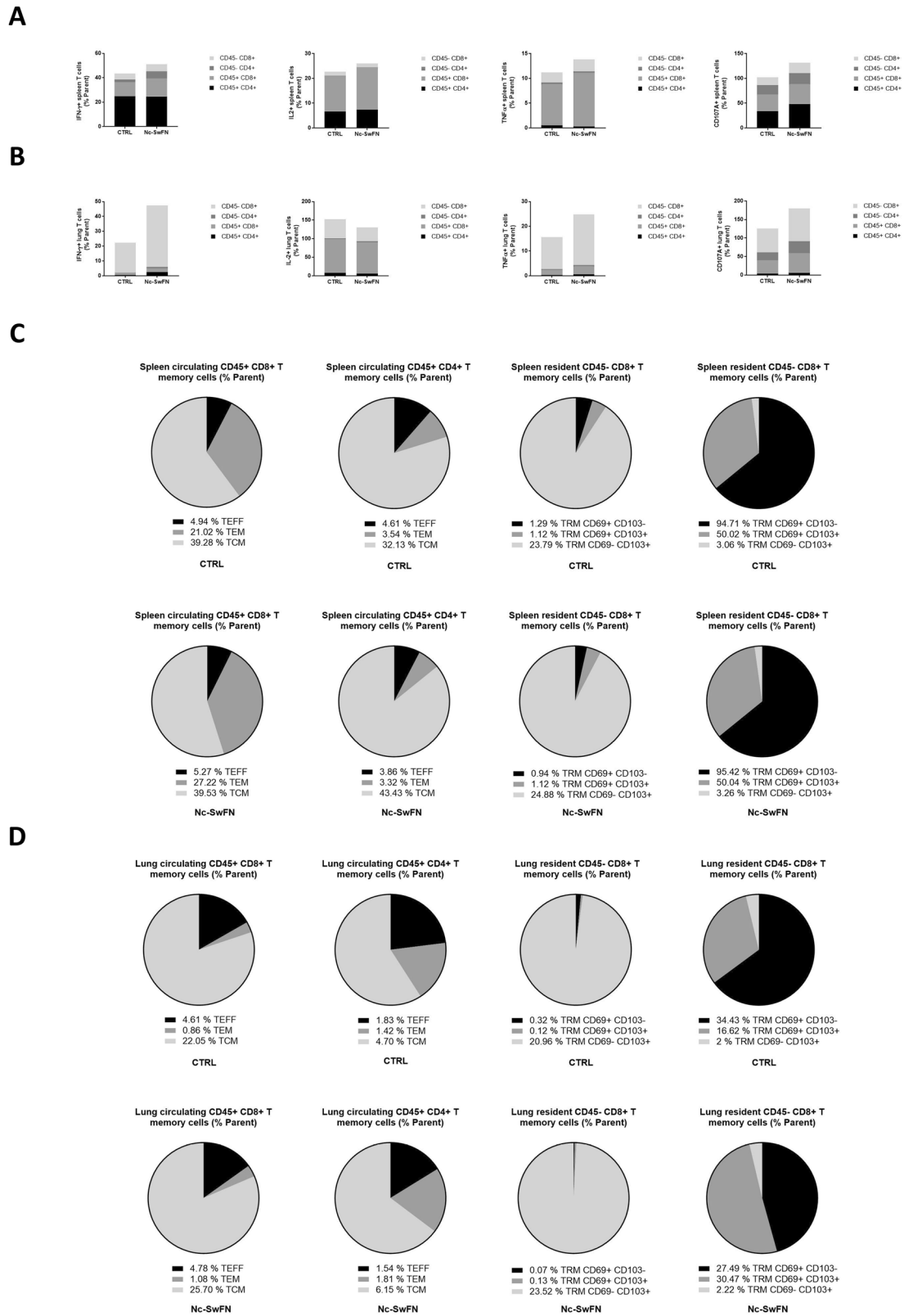
Fig. 5 | Circulating and tissue-resident effector and memory T-cell subsets in spleens and lungs of Nc-SwFN immunized mice. Female Balb/c mice were immunized twice at 3-week interval by intranasal route with Nc-SwFN complexation. Mice (*n* = 6 animals) were injected intravenously with anti-CD45-BV510 to distinguish circulatory and tissue-resident T cells. Intracellularly cytokine production (**A**, **B**) and T memory cell response (**C**, **D**) were analyzed in spleens and lungs, respectively. Gating strategies were showed in Supplementary figs. 4 and 5. Data were acquired on an MACSQuant®10 Analyzer (Miltenyi) and analyzed using FlowLogic software.
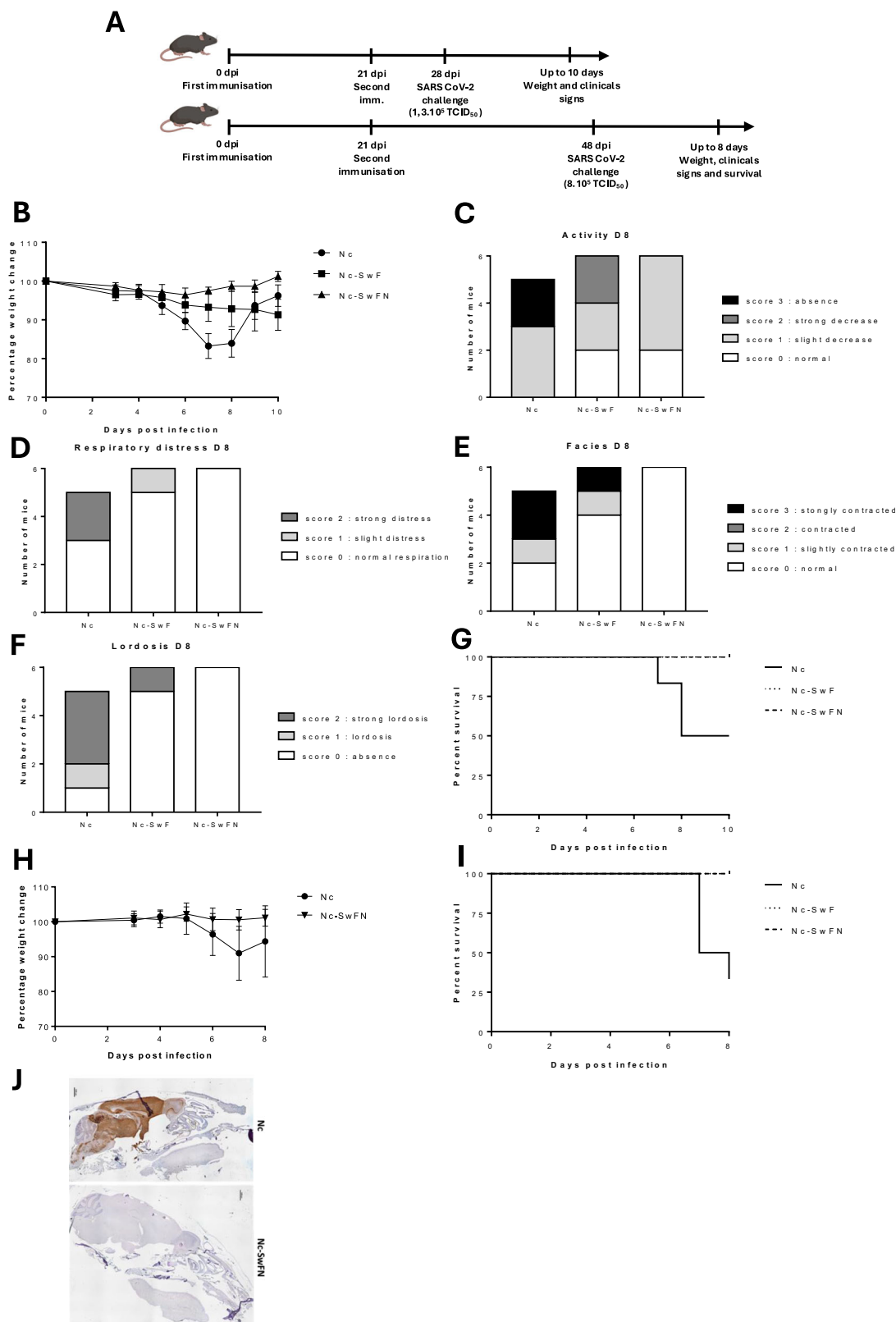
Fig. 6 | Evaluation of morbidity signs, survival mice, and virus presence after SARS-CoV-2 Delta infectious challenge. Female K18-hACE2 mice were immunized twice at 3-week interval by intranasal route, with nanocarriers alone (Nc) ($n = 6$ animals), Nc-SwF ($n = 6$ animals) or with Nc-SwFN complexation ($n = 6$ animals). One or 4 weeks after the second immunization, mice were infected with Delta SARS-CoV-2 variant. Experimental timelines were indicated in (**A**). Mice body weight was taken daily post-infection (**B**). After infection, different clinicals signs were observed daily. Mice activity (**C**), respiratory distress (**D**), facies (**E**), and lordosis (**F**) were presented on day 8 post-infection. Mice survival was showed after infection with 1.3×10^5 TCID$_{50}$ (**G**), and mice body weight and survival were showed after infection with 8×10^5 TCID$_{50}$ (**H**, **I**) of Delta SARS-CoV-2 variant. To evaluate virus presence, histological sections of head, from infected mice with Delta SARS-CoV-2 variant (8×10^5 TCID$_{50}$) since 7 or 8 days, were immunostained using SARS-CoV-2 N protein antibody (brown, scale bars: 1000 μm) ($n = 6$ heads for Nc and $n = 3$ heads for Nc-SwFN) (**J**). Survival data were analyzed by log-rank Mantel–Cox test (*$p < 0.05$, **$p < 0.01$).

mice maintained normal activity. For the two-thirds, only slight decrease in activity was observed in Nc-SwFN immunized mice, while Nc-SwF immunized mice even exhibited a strong decrease in activity (Fig. 6C). Furthermore, respiratory distress, contracted facies, and lordosis were observed in some mice of Nc control and Nc-SwF groups, while Nc-SwFN immunized mice were free of clinical symptoms (Fig. 6D–F). These results showed that Nc-SwFN vaccination protected K18-hACE2 mice against weight loss and morbidity after Delta SARS-CoV-2 variant infection. Compared to Nc-SwF, the absence of major clinical signs in Nc-SwFN mice highlighted the added value of the nucleoprotein protein. Up to 10 days post-infection with Delta SARS-CoV-2 variant (1.3×10^5 TCID$_{50}$), 50% mortality was observed in Nc group (Fig. 6G). One mouse died 6 days p.i., presenting a weight loss >15% and significant clinical signs: absence of activity, slight respiratory distress, strongly contracted facies, and strong lordosis (Data not shown). The two mice that died 8 days p.i. showed a major weight loss and the most important clinical signs. Whereas, no mortality was observed in the vaccinated groups, regardless of the vaccine protein.

To evaluate the Nc-SwFN vaccine extensive protection over time, survival and virus presence were analyzed 1 month post vaccination after a higher infectious dose (8×10^5 TCID$_{50}$) (Fig. 6A bottom). Seven days after infection with Delta SARS-CoV-2 variant, Nc control mice lost ~10% of their weight (Fig. 6H) and 66.7% of mortality was reached eight days after infection in Nc control group while all mice survived in the Nc-SwFN immunized group (Fig. 6I). Histological studies showed the presence of virus in the brain of two-thirds of the Nc control mice (olfactory bulb, cortex, cerebellum) whereas no virus was detected in the brains of Nc-SwFN immunized mice at 8 days p. i. (Fig. 6J). In addition to the effectiveness against morbidity, the Nc-SwFN vaccine candidate protected mice from mortality and virus presence in the brain.

Nc-SwFN vaccine protects Syrian hamsters from SARS-CoV-2 infection after direct challenge

The ability of Nc-SwFN vaccination to block virus multiplication and dissemination in the respiratory tract was evaluated using a susceptible hamster preclinical model.

Syrian hamsters were intranasally immunized with Nc and Nc-SwFN and further challenged by intranasal route 1 week after the last immunization with SARS-CoV-2 Delta variant. Serum and nasal anti-spike IgG and IgA were analyzed by ELISA, 7 days after the last immunization. Compared to the Nc control group, Nc-SwFN immunized animals produced a significantly higher amount of anti-spike IgG and IgA antibodies in serum and nasal washes (Supplementary Fig. 2A–E). Subsequently, the ability of these antibodies to neutralize SARS-CoV-2 virus (Wuhan and Delta strains) was tested. Total neutralization ability of serum from the Nc-SwFN group was observed against Wuhan and Delta strains respectively at a 1/80 and 1/160 dilution (Supplementary Fig. 2C). Nasal wash samples diluted at 1/5 indicated a neutralization capacity of mucosal antibodies from Nc-SwFN immunized animals as compared to control Nc, against both Wuhan and Delta SARS-CoV-2 strains (Supplementary Fig. 2F&G).

Prior to Delta strain SARS-CoV-2 infection, all animals were gaining weight at a similar rate (Data not shown). Two days after SARS-CoV-2 inoculation, Nc control group lost more weight than Nc-SwFN immunized group with a weight loss of -1.32 ± 0.58 as compared to -0.49 ± 0.97 (median ± IQR) (Fig. 7A). The level of viral RNA loads in the lung was significantly lower in Nc-SwFN immunized group as compared to Nc control group (Fig. 7B). In Nc control group, viral RNA load was detectable in three-quarters of animals with the variable level while all Nc-SwFN animals were below the limit of detection (Fig. 7B). Lung tissue obtained at 2 days p. i. was then explored for SARS-CoV-2 by immunochemistry and scoring (scoring method: Supplementary Table 2). SARS-CoV-2 nucleoprotein immunostaining was deeply extended in the lung parenchyma of Nc control animals with >25% of immunoreactive tissue in 3/4 animals and above 10% in the fourth control (Fig. 7C, D, Table S1). In contrast, SARS-CoV-2 nucleoprotein was undetected in the lung parenchyma of Nc-SwFN

immunized animals, and only one animal out of five showed a small focal staining restricted to the bronchoalveolar lumen (Fig. 7C, D, Table S1). Regarding the primary site of infection, the level of viral RNA load in the turbinates was significantly lower in Nc-SwFN immunized group as compared to Nc control group (Fig. 7E). Moreover, no viable SARS-CoV-2 virus was detected in the nasal swab of all Nc-SwFN immunized animals while three of four Nc control hamsters were positives (Fig. 7F). In a similar manner, SARS-CoV-2 nucleoprotein immunostaining of nasal cavity tissues in Nc control group showed extended immunostaining within proximal (naso and maxillary turbinates) and distal turbinates (Ethmoturbinates) with deep infiltrates from the epithelia to the parenchyma while the majority of Nc-SwFN immunized hamsters showed no or only focal immunostaining restricted to the epithelial surface of the turbinates (Fig. 7G, H).

All these results were reproduced following challenge with the Wuhan strain (Supplementary fig. 3) and confirmed the effectiveness of Nc-SwFN nasal vaccination in hamster's protection against SARS-CoV-2 infection by significantly reducing their viral load within the lung and the upper respiratory tract.
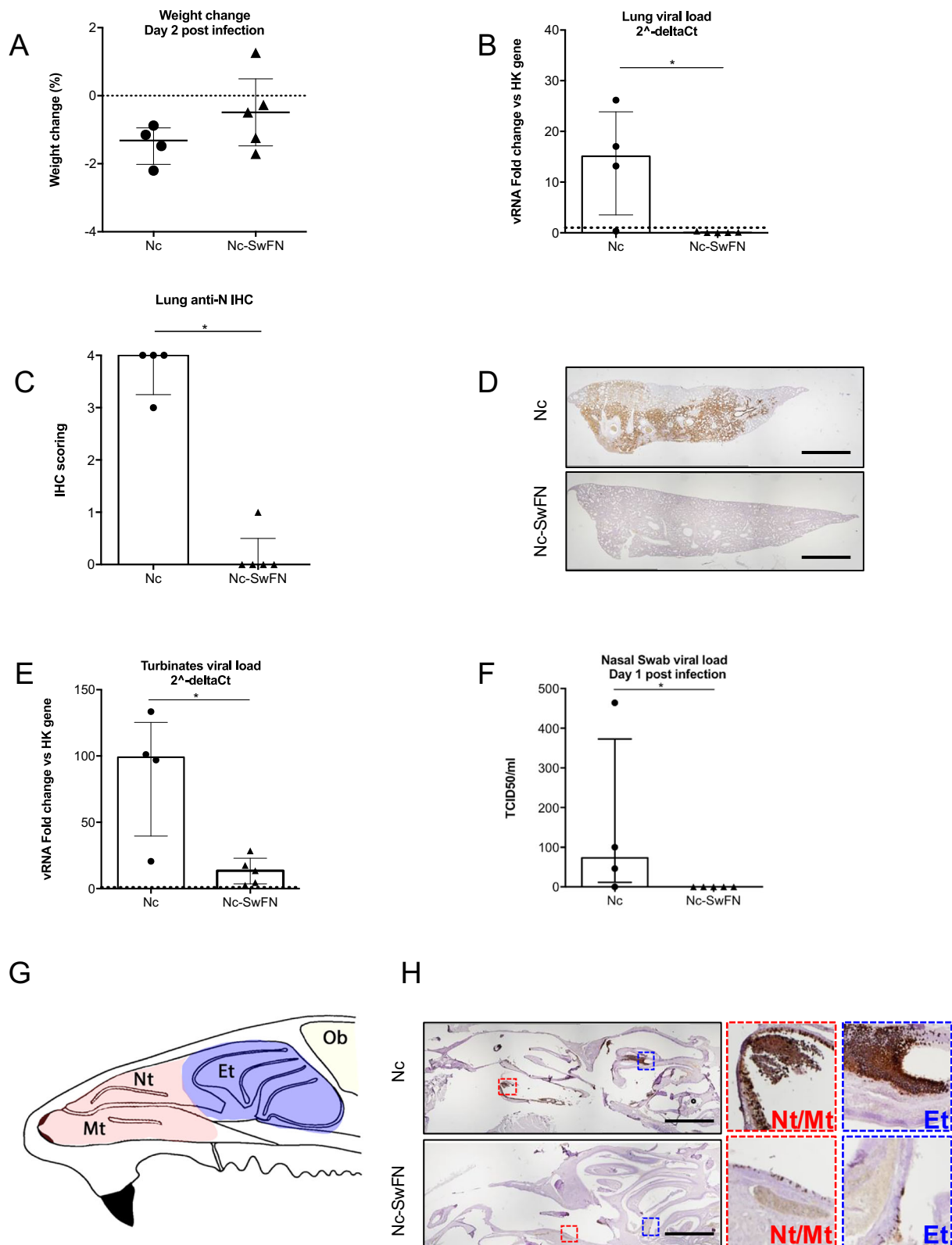
Nc-SwFN vaccine impairs SARS-CoV-2 transmission to naive hamsters

To evaluate the efficacy of vaccination to block contagiousness, naive sentinel hamsters were exposed to immunized and challenged animals with a ratio of 2:1 respectively. Maximal and optimized exposure were performed for 48 h, at the peak of viral shedding, between day 2 and 3 post infection (Fig. 8A) by co-housing the challenged animal in a new cage with two naive animals allowing airborne, direct contact, and potential fomite related transmission (Fig. 8A). The reliability of the transmissibility experiment was validated by comparison of Nc control versus Nc-SwFN challenged groups, to confirm the infectious status of Nc control group, with weight loss, viral load in the lung and nasal cavity (Fig. 8B–D) and TCID$_{50}$ analysis of the nasal swab (Fig. 8E).

Naive sentinel hamsters co-housed with animals from the Nc-SwFN immunized group (S-Nc-SwFN) did not show any significant weight loss with 9/10 animals maintaining their weight gain as compared to sentinel hamsters exposed to Nc challenged control group (S-Nc) where 7/10 animals stopped gaining weight (Fig. 8F). In this manner, 6/10 of the S-Nc lost weight and the statistical analysis of the weight comparison between S-Nc-SwFN and S-Nc data showed great significance (**<0.01, Fig. 8F). These results were correlated with the viral load in the lung. A very significant reduction of lung viral load was observed in S-Nc-SwFN group. Among the 10 S-Nc control group, 7 animals showed SARS-CoV-2 viral RNA within the lungs, while only one Nc-SwFN sentinel hamster had a low detectable lung viral load (**<0.01, Fig. 8G). Upstream of the lungs, the nasal cavity of the S-Nc-SwFN group showed a tendency of reduced viral load, as compared to the S-Nc control group (Fig. 8H). All the S-Nc groups showed SARS-CoV-2 viral RNA within the turbinates, whereas no trace of the viral RNA was detected in half of the S-Nc-SwFN hamster group (Fig. 8H). In accordance with the viral RNA level, TCID$_{50}$ analysis of viral load in the nasal swab after 2 days of co-housing confirms the significant reduction of transmission in S-Nc-SwFN hamsters. Among the 10 animals per group, only 4 S-Nc-SwFN hamsters showed detectable viral load as compared to 8 within the Nc control sentinels. Moreover, 4 out of 10 Nc control sentinels presented a high nasal viral load, over 100 TCID50/ml, thus becoming potential viral shedders (Fig. 8I). These data demonstrate that nasal Nc-SwFN immunization upstream SARS-CoV-2 infection impair virus transmission and resulted in significantly reduced lung and nasal turbinate viral load within naive unprotected sentinels allowing the blockage of the chain of contagion.

Discussion

The landscape of SARS-CoV-2 vaccine development has witnessed the emergence of numerous strategies, predominantly spike-based, aimed at preventing severe manifestations of the disease. However, these vaccines,

A. Weight change Day 2 post infection

B. Lung viral load 2^-deltaCt

C. Lung anti-N IHC

D. Nc / Nc-SwFN

E. Turbinates viral load 2^-deltaCt

F. Nasal Swab viral load Day 1 post infection

G. Ob, Et, Nt, Mt

H. Nc / Nc-SwFN — Nt/Mt, Et

administered intramuscularly, have shown limited efficacy against virus transmission and emerging variants. Addressing these limitations, our focus has been on developing an efficacious mucosal vaccine capable of impeding viral entry and transmission.

In response, we engineered a spike-Fc-nucleoprotein SARS-CoV-2 subunit vaccine (Nc-SwFN) integrated with biocompatible Ncs

demonstrating its ability to elicit protective immunity against SARS-CoV-2 morbidity, mortality, virus dissemination and transmission.

The electrostatic interaction between the negatively charged SwFN and positively charged maltodextrin Ncs facilitated multimerization, mimicking native virion morphology and enhancing vaccine immunogenicity. This formulation, akin to SARS-CoV-2 virus-like particles or outer membrane

Fig. 7 | Hamster protection associated with viral load abrogation in the lung and significant reduction in the nasal mucosa. Male golden hamsters were immunized twice at three-week interval by intranasal route, with nanocarriers alone (Nc) (n = 4 animals) and Nc-SwFN complexation (n = 5 animals). One week after the second immunization, all hamsters were infected 5×10^4 TCID$_{50}$ of SARS-CoV-2 Delta variant. Percentage of body weight change at day 2 post-infection compared to day 0 was presented in **A**. Lung tissues were collected at necropsy (day 2 post infection), and RNA was isolated for SARS-CoV-2 detection by qRT-PCR (**B**). Viral RNA relative loads compared to endogenous house-keeping control endogenous gene (2^(−deltaCt)) determined by qRT-PCR. A (2^(−deltaCt)) below 1 (dotted line) indicates no significant detection of viral RNA. For SARS-CoV-2 detection, lung tissues were processed for viral immunohistochemistry (IHC) using a mouse monoclonal anti-N antibody. Lung IHC scoring and representative images of lung sections IHC were showed in **C**, **D**, respectively. Ethmoid turbinates were collected at necropsy (day 2 post infection) and RNA was isolated for SARS-CoV-2 detection by qRT-PCR (**E**). Nasal swabs were collected on day 1 post-infection and infectious viral titers were determined by TCID50 (**F**). Schema of the hamster nasal cavity mucosa (Nt/Mt: Nasoturbinates and Maxilloturbinates, Et: Ethmoturbinates) (**G**). Representative images of nasal cavity mucosa viral IHC sections using a mouse monoclonal anti-N antibody (**H**). Higher magnification of Nt/mt and Et. The bars in the lung and nasal cavity figures represent 2 mm. Data were analyzed by a Mann–Whitney test (*$p < 0.05$).

vesicle-mC-Spike constructs, capitalized on maltodextrin Ncs' potential to enhance antigen absorption and stimulate mucosal immunity[10,13].

Contrary to soluble SwFN protein, complexation with mucosal Ncs potentiated humoral and cellular immune responses across systemic and mucosal compartments, notably amplifying IgA antibodies in nasal and BAL secretions.

The production of polymeric IgA in mucosal compartments has additional benefits against pathogen infiltration. The IgA multivalency forms resulted in greater avidity of viral peptides than IgG antibodies that might reduce viral load in the nose. The IgA antibodies were also known for their cross-protective activity against multiple strains[4,7,13]. In our study, the ability of mucosal antibodies to neutralize Wuhan and Delta strains has been observed. The induced antibody responses by spike-RBD mucosal vaccine also have the capacity to cross-neutralize multiple variants of concern[14,15]. The use of nucleoprotein had an added value in the enhancement of humoral spike-specific immunity.

The polymeric nature of mucosal IgA antibodies conferred broad cross-protective activity against multiple strains, including Wuhan and Delta variants. Nc-SwFN vaccine induced cross-reactivity against SARS-CoV-2 variants with spike and nucleoprotein-specific cellular immune responses. Spleen and lung cellular immune responses were characterized by IFN-γ, IL-2, and IL-17 cytokine production. The induction of a Th17-mediated immune response could contribute to the prevention of nasal cavity and lung pathogen colonization's[13,16]. Similar results were reported by Hajnik et al.[17] with the combination of spike-expressing mRNA clinical vaccine with mRNA-nucleoprotein.

Nasal vaccine effectiveness was often elevated owing to their capacity to induce T memory cells, especially in the respiratory system. Effector and memory T subset cell analysis following Nc-SwFN vaccination were in correlation with the literature[18]. Our results highlighted the principal role of spleen CD8+ TEM cells in the production of IFN-γ and TNF-α cytokines. However, IL-2 cytokine production in the spleen was mainly mediated by CD4+ TCM cells. In the lungs, TRM subset cells orchestrated the cytokine production. TRM cells represented immune sentinels at barrier sites that provided a stronger protective immunity than circulating T cells and can rapidly promote local and long-lasting protection against viral replication and transmission[19].

Few studies have demonstrated the potency of subunit spike protein-based vaccine to elicit potent T cell response by nasal route, but those always required the addition of an adjuvant as compared to our protocol based on a fusion protein solely formulated with a mucoadhesive carrier[14,15]. Nevertheless, the work from O'Neill et al., based on a protein Spike RBD domain boosted with the mucosal adjuvant mastoparan-7, showed promising enhanced T cell response by nasal administration as compared to the subcutaneous route for a similar dose of antigen, characterized by IFN$_\gamma$+/TNF$_\alpha$+ effector T cells with a high number of T$_{CM}$ cells[14].

Thereby, Nc-SwFN represents a polyvalent protective vaccine providing complementary immune defenses to clear SARS-CoV-2 viral infection. Protection efficiency has been confirmed on K18-hACE2 infection model using the widely spread and more virulent Delta SARS-CoV-2 variant for mice challenges[20–22]. No mortality was observed, and morbidity signs such as hunched appearance, restricted activity, respiratory distress, and contracted facies were almost non-existent in Nc-SwFN immunized K18-hACE2 mice. The more marked protection against Delta variant in Nc-SwFN as compared to Nc-SwF mice was probably due to the induced nucleoprotein-specific cellular immune response in accordance with the reported reduced sensitivity of Delta variant to antibody-neutralization[23]. Nc-SwFN mice protection was reinforced by the absence of mortality and virus presence in the cortex, cerebellum, and olfactory bulb, whereas all control mice with viral neuroinvasion were dead at 8 dpi as reported previously by Kumari et al.[24].

Prevention of virus dissemination in the lungs and the upper respiratory tract was also confirmed using the recognized standard pre-clinical Syrian hamster model[25,26]. Nc-SwFN vaccine against SARS-CoV-2 induced strong protection of the animals and showed a significant reduction of virus load in lung and nasal swab associated with a near complete protection of the lower and upper respiratory tract. The efficiency of Nc-SwFN vaccine to protect animals from Delta variant transmission was investigated with stringent challenge conditions. Sentinels were in direct contact with Nc control or Nc-SwFN vaccinated animals at the peak of shedding, implying a high transmission pressure by multiple routes from the challenged to the sentinel animals, including direct contact, fomites, and aerosols.

Nc-SwFN vaccine protects animals and impairs SARS-CoV-2 transmission to co-housed sentinels. S-Nc-SwFN had significantly reduced viral load in nasal swabs and no detectable virus RNA in the lung. Our results highlighted the protective role of local humoral immune response in the nasal cavity to block the viral access to the lower respiratory tract resulting in the absence of significant viral load in the lung. Indeed, we observed a drastically reduced viral load in the nasal cavity at early time points, between 1 and 3 days post-infection, although this period corresponded to the reported peak of viral load within these tissues in the hamster model[25,26]. Thereby, nasal Nc-SwFN vaccination, by preserving the lower respiratory tract from viral infection, not only provided strong protection for vaccinated animals but also impaired the virus transmission to unvaccinated animals, blocking the chain of transmission. As the nasal Nc-SwFN vaccine provided complementary immune defenses to clear and impair SARS-CoV-2 infection and transmission, it represents a broadspectrum vaccine solution against current and emerging SARS-CoV-2 variants.

Looking forward to the development of mucosal vaccines, this study paves the way for innovative approaches to respiratory infectious disease prevention. Only a mucosal and broadspectrum vaccine is able to, respectively, block virus at entry sites by inducing mucosal immune response and target multiple strains/variants.

Materials and methods
Ethics statement
All experiments were performed in accordance with European Guidelines for animal experimentation. The protocols were approved by the local ethics committee (CEEA Centre Val de Loire) and the French Ministry for Research. For immunogenicity experiments, animals were maintained under pathogen-free conditions in the animal facility of the University of Tours (PST-A). The infection experiments were performed in BSL-3 core facility (PFIE, INRAe Centre Val de Loire, France).

Fig. 8 | Nc-SwFN vaccine protection against viral transmission. Male golden hamsters were immunized twice at 3-week interval by intranasal route, with nanocarriers alone (Nc) ($n = 5$ animals) and Nc-SwFN complexation ($n = 5$ animals). One week after the second immunization, all hamsters were infected with 5×10^4 TCID$_{50}$ of SARS-CoV-2 Delta variant. To evaluate the impact of vaccination on viral transmission post infection, naive hamsters were co-housed for 48 hours with the challenged animals at a ratio of 2 sentinels for 1 challenged animal ($n = 10$ animals co-housed with the $n = 5$ Nc immunized & challenged animals and $n = 10$ animals co-housed with the $n = 5$ Nc-SwFN immunized & challenged animals). The experimental protocol was schematized in **A**. Percentage of body weight change at day 3 post-infection, or day 3 post co-housing, compared to day 0 in the challenged animals (**B**) and the sentinel animals (**F**). Lung tissues and ethmoid turbinates were collected at necropsy (day 3 post-infection or day 3 post co-housing), and RNA of challenged (**C**, **D**) and sentinel (**G**, **H**) animals was isolated for SARS-CoV-2 detection by qRT-PCR. Viral RNA relative load compared to endogenous house-keeping control endogenous gene ($2^{\wedge}(-\text{deltaCt})$) determined by qRT-PCR. A ($2^{\wedge}(-\text{deltaCt})$) below 1 (dotted line) indicates no significant detection of viral RNA. Nasal swabs were collected on day 1 and day 2 post-infection or co-housing, and infectious viral titers of challenged (**E**) and sentinel (**I**) animals were determined by TCID$_{50}$. Data were analyzed by a Mann–Whitney test (*$p < 0.05$; **$p < 0.01$).
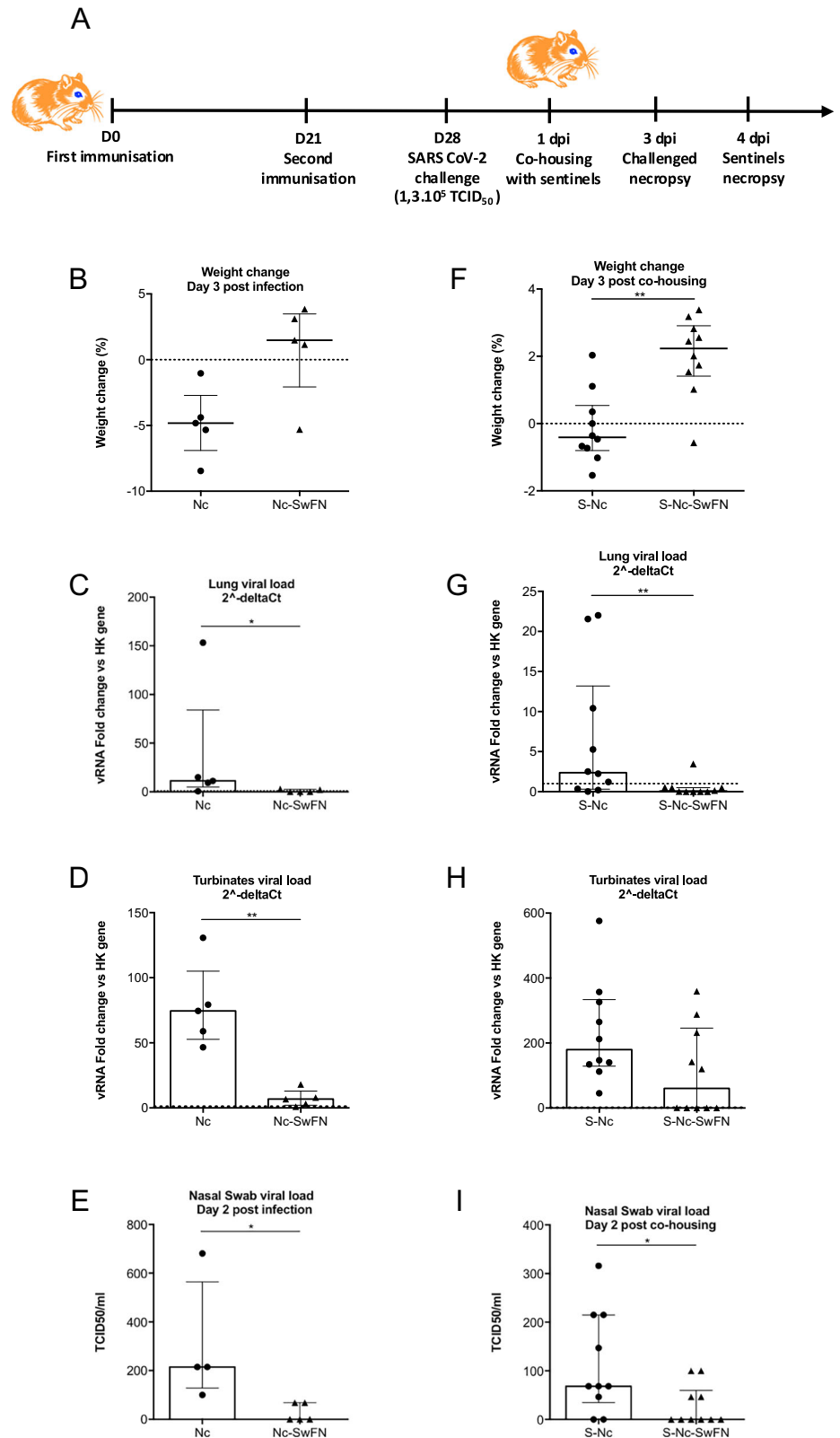
Virus isolation and preparation

Delta variant (B.1.617) was isolated from nasopharyngeal swabs collected from patients suffering from COVID-19 at the Tours University Hospital. The strain sequence was deposited on GISAID: B.1.617 strain EPI_ISL_16833396. Virus suspension (200 μL) was inoculated onto 12-well cell culture monolayers of Vero-TMPRSS2 cells which were previously maintained in Dulbecco's minimum essential medium (DMEM; Gibco, Scotland, UK) supplemented with 10% fetal bovine serum (FBS), 1.5 μg/ml puromycin (InvivoGen, San Diego, USA) penicillin (100 U/mL) and streptomycin (100 mg/mL). Cells were incubated for 1 hour at 37 °C to allow virus adsorption, with rocking every 10 min for uniform virus distribution. After incubation, the inoculum was removed, and the cells were washed

with 1× phosphate-buffered saline (PBS). The DMEM supplemented with 2% heat-inactivated FBS was added to each well. The cultures were incubated further in 5% CO_2 incubator at 37 °C and observed daily for cytopathic effect (CPE) under an inverted microscope (Olympus IX50). Five days later, supernatant was centrifuged at $4815 \times g$ for 5 minutes at 4 °C, and Tissue Culture Infective Dose 50% ($TCID_{50}$) quantitation was determined. $TCID_{50}$ values were calculated by the Reed and Muench method.

Protein design, production, and purification

The recombinant protein vaccine was a heteromultimeric spike-nucleoprotein fusion protein (SwFN). This fusion protein was obtained by co-transfection of two DNA plasmids. The first plasmid encodes a heavy chain (SwFN-hc) consisting of Wuhan spike protein ectodomain (GenBank accession number MN908947) with T4 foldon sequence[27], the hinge and CH2-CH3 domains of human IgG1 (IGHG1*01), followed by a peptide linker and the nucleoprotein sequence (GenBank accession number LR824570.1). The second plasmid encodes a light chain (Sw-lc) consisting of spike protein ectodomain with T4 foldon sequence and a C-tag (Thermo-Fisher Scientific). Thereby, the SwFN protein was composed of six Wuhan spike proteins, an Fc portion, and two nucleoproteins.

The spike sequences were modified to remove the polybasic cleavage site (mutation RRAR:A or R682del, R683del, and R685del), which is recognized by furin[28]. Furthermore, according to the HexaP variant described by Hsieh et al.[29], six other prolines were substituted to stabilize the prefusion conformation (mutations K986P, V987P) and to increase protein expression (mutations F817P, A892P, A899P, A942P).

To evaluate the added value of SARS-CoV-2 nucleoprotein, a control Wuhan spike protein in heteromultimeric form (SwF) was developed according to the same backbone sequence of the SwFN vaccine protein but without nucleoprotein sequence (SwF-hc and Sw-lc chains) and the induced immune response were compared to spike-nucleoprotein fusion protein.

For in vitro cell re-stimulation, spike from Wuhan (Sw), Delta (Sd) (B.1.617.2, GenBank N° MZ208926), and Omicron (So) (B.1.1.529, GenBank N° OW996240.1) strains were produced. The ectodomain sequence of each strain was fused to a T4 foldon sequence followed by the C-tag.

Spike-T4 foldon, nucleoprotein and Fc sequences with optimized codons for *Cricetulus griseus* were synthesized by GeneArt in pcDNA3.4 plasmid. Specific sequences of interest were amplified by specific PCR primers and were then integrated in pcDNA3.4 plasmid with the BsaI-HF v2 Golden Gate technology (New England Biolabs). Final constructions (pcDNA3.4-Sw-lc, pcDNA3.4-Sd-lc, pcDNA3.4-So-lc, pcDNA3.4-SwF-hc, pcDNA3.4-SwFN-hc) were purified and validated by sequencing analysis. High-quality DNA Plasmids from DH5 bacteria were performed (QIAGEN Plasmid Maxi Kit) and used for ExpiCHO-S cell line transfection according to the manufacturer's instructions (ThermoFisher Scientific). Briefly, CHO cells were previously diluted at 6×10^6 cells/mL, and ExpiFectamine-DNA plasmid complexes were added. For spike proteins (Sw, Sd, and So), 0.8 µg/mL of DNA plasmid was used. For SwF and SwFN proteins, a ratio of 3:1 (corresponding respectively to 0.6 µg/mL of pcDNA3.4-SwFN-hc and 0.2 µg/mL pcDNA3.4-Sw) was used. Max titer protocol was applied, and supernatants were harvested after 8 days post-transfection when cell viability was greater than 60% (CytoSMART, Corning). Clarified supernatants were obtained after centrifugation at $10,000 \times g$ for 10 min and stored at −20 °C until purification.

Before purification, supernatants were clarified again by centrifugation at $10,000 \times g$ for 20 min followed by 0.22 µm filtration. Protein purification was performed with an Akta purifier (GE Healthcare Europe GmbH) using specific columns for affinity chromatography. HiTrap HP protein A column (Cytiva) was used for heteromultimeric protein purification (SwF and SwFN). The column was equilibrated with PBS (2.7 mM KCl, 0.14 M NaCl, 1.5 mM KH2PO4, 8 mM Na2HPO4, pH 7.4), and bound proteins were eluted after PBS washing with citrate buffer (100 mM, pH 3). Capture Select C-tagXL column (Cytiva) was used to purify spike proteins (Sw, Sd, and So). The column was equilibrated with 20 mM Tris at pH 7.5, unspecific proteins were eliminated with wash buffer (20 mM Tris pH 7.5, 1 M NaCl), and

specific C-tag proteins were eluted with citric acid buffer (100 mM, pH 3). Afterwards, a desalting column (HiPrep 26/10 desalting column Cytiva) was used for elution buffer exchange into PBS. Protein concentration was determined with a UV detector at 280 nm. Molecular mass and molar extinction coefficient data were generated by the Protparam tool from http://web.expasy.org/protparam/. Proteins were concentrated with 30 kD Amicon Ultra (Merk Millipor) at 1 mg/mL, sterilized by 0.22 µm filtration and stored at 4 °C.

Prometheus NT.48 was used to measure the thermal unfolding profiles of proteins by differential scanning fluorimetry experiments (Prometheus NT.48, NanoTemper). All samples were used at a final concentration of 1 µM and loaded into high-sensitivity capillaries (Nanotemper). The protein unfolding process was subjected to a thermal ramp (20–95 °C, 1 °C/min). Data analysis involved using Prometheus PR ThermControl software. The Tm value was determined by fitting the tryptophan 350/330 nm fluorescence emission ratio using a polynomial function in which the maximum slope is indicated by the peak of its first derivative.

Antigenicity of produced proteins was studied using anti-N sandwich enzyme-linked immunosorbent assay (ELISA). Flat-bottomed 96-well plates (Nunc) were coated with human anti-SARS-CoV spike Protein S1 Receptor-Binding Domain Antibody (1:1000, 100-0583, Stemcell). Serial two-fold dilutions of SwFN fusion protein, Sw, SwF, and irrelevant protein were performed (starting at 300 µg/mL) and added to the wells. SwFN was detected using anti-SARS-COV-2 Nucleoprotein antibody (1:5000, Stemcell, 100-0580) followed by an IgG (H + L) Cross-Adsorbed F(ab′)2-Goat anti-Rabbit, AP (1:2500, Invitrogen, 15440954). The optical density of each point was read at 405 nm.

Mucosal Nc preparation

The Nc were synthesized according to Dombu et al.[30]. The maltodextrin (Glucidex from Roquette, France) was dissolved in a 2 N sodium hydroxide solution with magnetic stirring at room temperature, then epichlorohydrin and glycidyl trimethyl ammonium chloride (Sigma-Aldrich, France) were added, leading to the formation of a cationic hydrogel. The gel was then neutralized with acetic acid and crushed by a high-pressure homogenizer (LM20-30 microfluidizer, Microfluidics, France). The Nc were purified over ultrapure water by tangential flow ultra-filtration (Akta Flux6, GE Healthcare, France) using a 300 kDa cutoff hollow fiber and filtered through 0.2 µm.

Vaccine preparation and characterization

Hetero-multimeric spike protein (SwF) and heteromultimeric fusion protein (SwFN) were complexed with Nc at a 3:1 mass ratio (Nanocarriers:Protein) to obtain SwF (Nc-SwF) and SwFN (Nc-SwFN) complexations, respectively. Ncs were mixed with antigen for 1 hour at room temperature under shaking conditions. Water volume was adjusted, and vaccine preparations were stored at 4 °C for 24 h–48 h before use. For immunogenicity and survival experiments in BALB/c and K18-hACE2 mouse models, each mouse was immunized with an equimolar quantity corresponding to 10 µg of spike protein (73.6 pmol). For Nc-SwF complexation, 31.8 µg of Ncs were mixed with 10.6 µg of SwF, and 35.4 µg of Ncs were mixed with 11.8 µg of SwFN to obtain Nc-SwFN complexation. For protection and contagiousness experiments in hamster model, each animal received the equivalent of 50 µg (368 pmol) of spike protein, either a mix of 176.4 µg of nanoparticles and 58.8 µg of SwFN.

Protein complexations (~5 µg of protein) were analyzed using native polyacrylamide gel electrophoresis (PAGE) with silver staining according to the manufacturer's instructions (Fisher Scientific). SwFN vaccine complexation was analyzed using formvar/carbon-coated nickel grids. TEM imaging was performed with JEOL microscope (1011, Tokyo, Japan) after negative staining with three consecutive contrasting steps using phosphotungstic acid (IBiSA electronic microscopy platform of Tours University). Vaccine local penetration and internalization by the human nasal mucosa were performed in vitro on MucilAir™ cell model of the human airway epithelium (Epithelix) after Nc-SwFN (50 µg/mL) incubation for 30 mins

and 6 hours, respectively. Cells were scrapped, fixed, dehydrated, and embedded in Epon resin (Sigma). Ultra-thin sections (90 nm) were obtained with a Leica EM UC7 ultramicrotome (Wetzlar, Germany) and sections were stained with 5% uranyl acetate (Agar Scientific), 5% lead citrate (Sigma). TEM observations were made with JEOL microscope (1011, Tokyo, Japan).

Animal experiments
Animal were housed in an SPF BSL2/3 animal facility under classical light/dark cycle and temperature and where feed ad libitum with fresh water and complete maintenance diet (SAFE A04, Safe-lab, Germany) with bedding and environmental enrichment consisting of shredding paper and plastic igloo available in the cage.

Mice immunizations
BALB/c immunogenicity. Six-week-old female BALB/c mice obtained from CER Janvier (Le Genest Saint Isle, France), were used for immunogenicity experiments. Groups of six mice were immunized twice by intranasal route at 3-week intervals with 20 μL of Ncs alone, SwFN fusion protein, Nc-SwF and Nc-SwFN complexations. Vaccine immunogenicity was evaluated 1 week after the 2nd dose by studying systemic and mucosal immune responses.

K18-hACE2 clinical signs and survival. Eight-week-old female K18-hACE2 mice obtained from Charles River (Saint-Germain-Nuelles, France) were used to study clinical signs and survival after SARS-CoV-2 infection following vaccination. Groups of six mice were immunized with Nc alone, Nc-SwF, and Nc-SwFN complexations. Each group was immunized twice at 3-week intervals by intranasal inoculation. Following immunization and before infection, the serum anti-spike antibody response was analyzed by ELISA. Mice were infected one week after the second immunization with a sublethal dose of 1.3×10^5 TCID$_{50}$ Delta SARS-CoV-2 variant (20 μL) in order to study the appearance of clinical signs. For the survival study, mice were infected four weeks after the second immunization with a lethal dose of 8×10^5 TCID$_{50}$ Delta SARS-CoV-2 variant (30 μL). The infectious challenge was performed intranasally, under isoflurane anesthesia. The mice were weighed once a week before infection. Following infection, weight, clinical signs (activity, respiratory distress, lordosis, contracted facies), and survival were assessed daily. Mice were sacrificed by isoflurane overdose followed by cervical dislocation, 10- and 8 days post-infection, respectively, for clinical signs and survival studies. Lung, nasal cavity, olfactory bulb, and brain sections were analyzed by immunohistology.

Hamster immunizations
Four-five-week-old male golden hamsters, chosen for their higher gender susceptibility to the SARS-CoV-2 virus[31,32], were obtained from CER Janvier (Le Genest Saint Isle, France). For the protection study, four hamsters received Nc alone, and five hamsters were immunized with Nc-SwFN complexation under isoflurane anesthesia and following a protocol of two intranasal inoculations separated by 3 weeks. Hamsters were challenged via an intranasal route with 5×10^4 TCID$_{50}$ of SARS-CoV-2 Delta variant (80 μL) under isoflurane anesthesia. Body weights were monitored daily. Viral load in lung and nasal swab were analyzed 2 days post-infection by real-time quantitative reverse transcription PCR (qRT-PCR) and TCID$_{50}$, respectively. Lung sections were also prepared for analysis by immunohistology.

To evaluate the efficacy of vaccination against SARS-CoV-2 infection and transmissibility by direct contact, 30 hamsters were divided into 10 experimental groups of three animals originating from the same litters to allow serene co-housing. Five hamsters were previously immunized with two intranasal doses (80 μL) of Nc alone or Nc-SwFN complexation at 3 weeks of interval. Hamsters were then challenged 1 week post vaccination via intranasal route with 5×10^4 TCID$_{50}$ of SARS-CoV-2 Delta variant under isoflurane anesthesia. One day post infection, each Nc or Nc-SwFN

vaccinated / infected hamster was transferred back to cohouse for 48 hours, corresponding to previously reported pic of viral shedding, with two naive sentinel hamsters in a new cage allowing both airborne movement, direct contact, and potential fomite transmission to maximize and optimize the contagiousness[26]. Body weights were monitored daily. At the end of the experiments, hamsters were sacrificed by isoflurane overdose, followed by decapitation. Viral load in lung, olfactive mucosa were analyzed by qRT-PCR and nasal swab by TCID$_{50}$. Lung sections were also prepared for analysis by immunohistology.

Humoral immune response analysis
Analyses of spike-specific IgG and IgA antibodies were performed by ELISA on serum, nasal and bronchoalveolar washes, collected 1 week after the last immunization. Flat-bottomed 96-well plates (Nunc) were previously coated with 2 μg/mL of spike from Wuhan strain (Sw). To determine respectively endpoint titers and optical density (OD), serial two-fold dilutions (starting at a 1:50 dilution) of serum and pure nasal or BAL washes were performed and added to the wells after plate saturation. Sample of Nc immunized mice served as negative control. For mouse models, goat anti-mouse IgG alkaline phosphatase (1:5000, A3438 Sigma) and goat anti-mouse IgA alkaline phosphatase conjugate (1:1000, A4937 Sigma) were used to detect bound antibodies. For hamster model, IgG and IgA antibodies were detected using goat anti-hamster IgG alkaline phosphatase (1:5000, Sab37700489 Sigma) and rabbit anti-hamster IgA alkaline phosphatase conjugate (1:1,250, Sab 3005 Brookwood Medical). The optical density of each sample was read at 405 nm, and the endpoint antibody titer for each sample was given as the reciprocal of the highest dilution, producing an OD that was 2.5-fold greater than that of the serum of naive mice. Antibody neutralization capacities were evaluated by mCherry SARS-CoV-2 RT-PCR and plaque reduction neutralization tests (PRNT) analysis.

All neutralization experiments were performed in a biosafety level 3 laboratory. The different viral strains that were used were sequenced and deposited on GISAID [GISAID accession numbers: EPI_ISL_1707038, 19 A (B.38); EPI_ISL_1904989, Delta (B.1.617.2); and EPI_ISL_7608613, Omicron (B.1.1.529)]. Neutralization tests were performed as previously described[33]. Briefly, Decomplemented serum specimens were tested in duplicate at serial 2-fold dilutions from 1/10. Nasal washes and LBA were tested individually in duplicates against Delta and pooled against Wuhan. For the nasal washes and LBA, the percentage of neutralization was estimated only at the dilution of 1/5 and scores of neutralizations were categorized as follow: negative: <20% neutralization; Low : 20-40% neutralization; intermediate : 40–60% neutralization and high : >60% neutralization. The samples were mixed at equal volume with the live SARS-CoV-2 virus. After incubation of the mix for 30 min at room temperature, 150 μL of the mix was transferred into 96-well microplates covered with a monolayer of Vero E6 cells to achieve a viral concentration of 100 TCID$_{50}$/well. The plates were incubated at 37 °C in a 5% CO2 atmosphere for 5 days. For RT-PCR analysis, SARS-CoV-2 was quantified in the culture supernatant directly without nucleic acid extraction, with the Luna Universal Probe One-Step RT-qPCR Kit (New England Biolabs). Briefly, 5 μL of supernatant was diluted 1/10 with Dnase-free and Rnase-free water and mixed with the reaction solution to obtain a total volume of 14 μL. The reaction solution contained 5 μL Luna® Universal Probe One-Step Reaction Mix, 0.5 μL Luna® WarmStart® RT Enzyme Mix and 1.5 μL of a mixture of primers at 400 nM (E_Sarbeco_F: ACAGGTACGTTAATAGTTAATAGCGT and E_Sarbeco_R: ATATTG-CAGCAGTACGCACACA) and the probe at a concentration of 200 nM (E_Sarbeco_P1: FAM-ACACTAGCCATCCTTACTGCGCTTCG-BBQ). The RT-PCR was initialized with a reverse transcription step at 55 °C for 10 min, followed by 40 cycles of denaturation at 95 °C for 10 s and annealing at 60 °C for 60 s. A viral standard curve was obtained for each analysis to calculate the neutralization percentage. For PRNT analysis, the CPE was evaluated after 5 days, and neutralization was recorded if less than 50% of the cells were damaged. The results were presented as very weak, weak and visible neutralizations.

Article

Cellular immune response analysis

Systemic and mucosal cellular immune responses were analyzed one week after the last immunization in order to evaluate the produced cytokines and the functional signature of T cells. Spleen cell suspensions were individually obtained by filtration through nylon mesh. Lungs were harvested using a Lung dissociation kit (Miltenyi Biotec) according to the manufacturer's instructions. Erythrocytes were removed by lysis (hypotonic shock), and the remaining cells were washed and suspended in RPMI 1640 medium supplemented with 5% FCS, 25 mM HEPES, 2 mM L-glutamine, 1 mM sodium pyruvate, 50 μM β-mercaptoethanol, 100 U/mL penicillin, and 100 μg/mL streptomycin. Cytokine production was analyzed in the supernatant of the spleen and lungs. 5×10^5 cells were stimulated with 10 μg/mL of spike variants (Sw, Sd, and So) or Nucleoprotein (230-30164, Clinisciences). Cytokine productions were analyzed after 72 hours using Mouse MACsPlex cytokine Kit (Miltenyi Biotec) according to the manufacturer's instructions. Intracellular T-cell cytokine production was also measured. To distinguish circulatory and tissue-resident T cells, BALB/c mice were injected intravenously with 3 μg of anti-CD45-BV510 (clone 30-F11, Biolegend) and were euthanized 3 min later. Cells were incubated for 4 h in a complete medium containing Golgi stop (BD) and anti-CD107-FITC (1:100, BD). Stimulated cells were stained with VioBlue Dye 405-452 (1:100, Miltenyi Biotec), anti-CD8a-Pacific blue (1:2000, clone 53-6.7, Biolegend) and anti-CD4-PE-Cy5.5 (1:160, clone RM4-5, eBioscience) in FACS-PBS for 20 min at 4 °C. After fixation (cytofix, 20 min, 4 °C) and permeabilization (Permwash 1×, 4 °C), cells were stained intracellularly with anti-IL-2-APC (1:300, clone JES6-5H4, Biolegend), anti-TNF-PE-Cy7 (1:300, clone MPG-XT22, Biolegend), and anti-IFNy-PE (1:300, clone XMG1.2, Biolegend). Data were acquired on a MACSQuant®10 Analyzer (Miltenyi Biotec) and analyzed using FlowLogic software.

T memory cell response has been further analyzed. Stimulated cells were stained in FACS-PBS with anti-CD44-APC (1:5000, clone IM7, BioLegend), anti-CD8-BV421 (1:40, clone 53-6.7, BioLegend), anti-CD4-BV510 (1:40, clone RM4-5, BioLegend), anti-CD127-FITC (1:500, clone A7R34, BioLegend), anti-KLRG1-PE-Cy7 (1:80, clone 2F1, eBioscience), anti-CD127-FITC (1:500, clone A7R34, BioLegend), anti-CD69-PerCP-Cy5.5 (1:300, clone H1.2F3, BioLegend) and anti-CD103-PE (1:200, clone 2E7, eBioscience). Data were acquired on a MACSQuant®10 Analyzer (Miltenyi Biotec) and analyzed using FlowLogic software.

Viral load analysis

SARS-CoV-2 RNA quantitative real-time RT-PCR. Lung and olfactory mucosae (Etmoid turbinates of one side of the head of the hamster) biopsies were removed aseptically and frozen at −80 °C. Samples were thawed and homogenized in lysing matrix M (MP Biomedical) using a Precellys 24 tissue homogenizer (Bertin Technologies). The homogenates were centrifuged 10 min at $2000 \times g$ for further RNA extraction from the supernatants using the RNeasy mini kit (Qiagen) following manufacturer's instructions. SARS-COV-2 RNA quantitative real-time RT-PCR detection was further performed using the ID gene SARS-COV-2 Duplex kit (ID.Vet, Innovative Diagnostics) according to the manufacturer's procedure. Quantitative RT-PCR was performed and analyzed using a LightCycler 96® Instrument (Roche Life Science).

SARS-CoV-2 TCID$_{50}$ assay. Collected nasal swab were frozen at −80 °C in cell medium for further TCID$_{50}$ assay in Vero cells. Samples were thawed and tittered using the Tissue Culture Infectious Dose 50 Assay (TCID$_{50}$/ml) system. Vero cells were plated the day before infection into 96-well plates at 1.5×10^4 cells/well. On the day of the experiment, serial dilutions of the virus were made in media, and a total of six wells were infected with each serial dilution of the virus (with a starting dilution of 1:5 for the swab). After 48 h incubation, cells were fixed in 4% paraformaldehyde (PFA) followed by staining with 0.1% crystal violet. The TCID$_{50}$ was then calculated using the formula: $\log(TCID_{50}) = \log(do) + \log(R)(f+1)$. Where do represents the dilution giving a positive well, f is a number derived from the number of positive wells calculated by a moving average, and R is the dilution factor.

Immunohistology. Lungs were fixed in 4% PFA 72 h and were processed for paraffin embedding, and 4–5 μm sections were used for immunohistochemistry. Half of the animal head was fixed for 3 days at room temperature in 4% PFA PBS, then decalcified for 3 days (10% EDTA–pH 7.3 at 4 °C). For mice model, immunohistochemistry was performed using anti-SARS-CoV-2 nucleoprotein antibody (1:500, GTX135357, Clinisciences). Followed by goat HistoFine anti-RABBIT (70%) and HRP revelation (DAB quanto, Thermofisher). For hamster model, the nasal septum and endoturbinates were selected as a block for convenient focus on the nasal cavity for further viral scoring following immunohistochemistry (see below). SARS-CoV-2 nucleoprotein was detected using mouse monoclonal antibody (1C7C7). The Histofine Simple Stain Mouse MAX PO kit was used as the secondary anti-mouse HRP (Nichirei Biosciences inc.). Images were captured using a Nikon Eclipse 80i microscope with DS-Ri2 camera controlled by the NIS-Elements D software package (Nikon, Instruments Inc., Tokyo, Japan).

Statistical tests

Statistical analyses were performed with Prism 7.0 (GraphPad Software, Inc.) and were done by one or two-way ANOVA or nonparametric analysis followed by a Dunn's multiple or Kruskal–Wallis comparison tests. Results are shown as mean ± SEM (one-way ANOVA test) or as median ± interquartile range (Kruskal–Wallis test). Survival statistics were performed with the log-rank Mantel–Cox test. A $p < 0.05$ was considered to be statistically significant.

Data availability

All data generated or analyzed during this study are included in this manuscript. All relevant data are available from the authors.

References

1. Belete, T. M. Review on up-to-date status of candidate vaccines for COVID-19 disease. *IDR ume* **14**, 151–161 (2021).
2. Hadj Hassine, I. Covid-19 vaccines and variants of concern: a review. *Rev. Med. Virol.* **32**, e2313 (2022).
3. A. M. Carabelli, et al. SARS-CoV-2 variant biology: immune escape, transmission and fitness. *Nat. Rev. Microbiol.* https://doi.org/10.1038/s41579-022-00841-7 (2023).
4. Travis, C. R. As Plain as the nose on your face: the case for a nasal (Mucosal) route of vaccine administration for Covid-19 disease prevention. *Front. Immunol.* **11**, 591897 (2020).
5. Tiboni, M., Casettari, L. & Illum, L. Nasal vaccination against SARS-CoV-2: synergistic or alternative to intramuscular vaccines? *Int. J. Pharm.* **603**, 120686 (2021).
6. Dhama, K. et al. COVID-19 intranasal vaccines: current progress, advantages, prospects, and challenges. *Hum. Vaccin. Immunother.* **18**, 2045853 (2022).
7. Sterlin, D. et al. IgA dominates the early neutralizing antibody response to SARS-CoV-2. *Sci. Transl. Med.* **13**, eabd2223 (2021).
8. Wang, Z. et al. Enhanced SARS-CoV-2 neutralization by dimeric IgA. *Sci. Transl. Med.* **13**, eabf1555 (2021).
9. Bernocchi, B., Carpentier, R. & Betbeder, D. Nasal nanovaccines. *Int. J. Pharm.* **530**, 128–138 (2017).
10. Vu, M. N., Kelly, H. G., Kent, S. J. & Wheatley, A. K. Current and future nanoparticle vaccines for COVID-19. *eBioMedicine* **74**, 103699 (2021).
11. Joag, V. et al. Cutting edge: mouse SARS-CoV-2 epitope reveals infection and vaccine-elicited CD8 T cell responses. *J. Immunol.* **206**, 931–935 (2021).
12. Lamichhane, A., Azegami, T. & Kiyono, H. The mucosal immune system for vaccine development. *Vaccine* **32**, 6711–6723 (2014).
13. Van Der Ley, P. A., Zariri, A., Van Riet, E., Oosterhof, D. & Kruiswijk, C. P. An intranasal OMV-based vaccine induces high mucosal and

systemic protecting immunity against a SARS-CoV-2 infection. *Front. Immunol.* **12**, 781280 (2021).

14. O'Neill, A. et al. Mucosal SARS-CoV-2 vaccination of rodents elicits superior systemic T central memory function and cross-neutralising antibodies against variants of concern. *eBioMedicine* **99**, 104924 (2024).

15. Kingstad-Bakke, B. et al. Vaccine-induced systemic and mucosal T cell immunity to SARS-CoV-2 viral variants. *Proc. Natl Acad. Sci.* **119**, e2118312119 (2022).

16. Raeven, R. H. M. et al. Intranasal immunization with outer membrane vesicle pertussis vaccine confers broad protection through mucosal IgA and Th17 responses. *Sci. Rep.* **10**, 7396 (2020).

17. Hajnik, R. L. et al. Dual spike and nucleocapsid mRNA vaccination confer protection against SARS-CoV-2 Omicron and Delta variants in preclinical models. *Sci. Transl. Med.* **14**, eabq1945 (2022).

18. Ahlers, J. D. & Belyakov, I. M. Memories that last forever: strategies for optimizing vaccine T-cell memory. *Blood* **115**, 1678–1689 (2010).

19. Alu, A. et al. Intranasal COVID-19 vaccines: from bench to bed. *eBioMedicine* **76**, 103841 (2022).

20. Oladunni, F. S. et al. Lethality of SARS-CoV-2 infection in K18 human angiotensin-converting enzyme 2 transgenic mice. *Nat. Commun.* **11**, 6122 (2020).

21. Liu, X. et al. The delta SARS-CoV-2 variant of concern induces distinct pathogenic patterns of respiratory disease in K18-hACE2 transgenic mice compared to the ancestral strain from Wuhan. *mBio* **13**, e00683–22 (2022).

22. Wong, T. Y. et al. Evaluating antibody mediated protection against alpha, beta, and delta SARS-CoV-2 variants of concern in K18-hACE2 transgenic mice. *J. Virol.* **96**, e02184–21 (2022).

23. Planas, D. et al. Reduced sensitivity of SARS-CoV-2 variant Delta to antibody neutralization. *Nature* **596**, 276–280 (2021).

24. Kumari, P. et al. Neuroinvasion and encephalitis following intranasal inoculation of SARS-CoV-2 in K18-hACE2 mice. *Viruses* **13**, 132 (2021).

25. Chan, J. F.-W. et al. Simulation of the clinical and pathological manifestations of coronavirus disease 2019 (COVID-19) in a golden syrian hamster model: implications for disease pathogenesis and transmissibility. *Clin. Infect. Dis.* **71**, 2428–2446 (2020).

26. Sia, S. F. et al. Pathogenesis and transmission of SARS-CoV-2 in golden hamsters. *Nature* **583**, 834–838 (2020).

27. Meier, S., Güthe, S., Kiefhaber, T. & Grzesiek, S. Foldon, the natural trimerization domain of T4 fibritin, dissociates into a monomeric a-state form containing a stable β-hairpin: atomic details of trimer dissociation and local β-hairpin stability from residual dipolar couplings. *J. Mol. Biol.* **344**, 1051–1069 (2004).

28. Wang, Q. et al. A unique protease cleavage site predicted in the spike protein of the novel pneumonia coronavirus (2019-nCoV) potentially related to viral transmissibility. *Virol. Sin.* **35**, 337–339 (2020).

29. Hsieh, C.-L. et al. Structure-based design of prefusion-stabilized SARS-CoV-2 spikes. *Science* **369**, 1501–1505 (2020).

30. Dombu, C., Carpentier, R. & Betbeder, D. Influence of surface charge and inner composition of nanoparticles on intracellular delivery of proteins in airway epithelial cells. *Biomaterials* **33**, 9117–9126 (2012).

31. Yuan, L. et al. Gender associates with both susceptibility to infection and pathogenesis of SARS-CoV-2 in Syrian hamster. *Sig. Transduct. Target Ther.* **6**, 136 (2021).

32. Castellan, M. et al. Host response of Syrian Hamster to SARS-CoV-2 infection including differences with humans and between Sexes. *Viruses* **15**, 428 (2023).

33. Pozzetto, B. et al. Immunogenicity and efficacy of heterologous ChAdOx1–BNT162b2 vaccination. *Nature* **600**, 701–706 (2021).

Author contributions
Z.L. produced and characterized the fusion protein, performed the complexation of vaccine protein with Ncs, designed BALB/c mouse studies, performed the experiments, analyzed and interpreted the data, contributed to K18-hACE2 mouse and hamster studies, wrote, critically revised, and edited the manuscript. A.P.B. performed the complexation of vaccine protein with Ncs, designed K18-hACE2 studies, performed the experiments, analyzed and interpreted the data, contributed to BALB/c mouse and hamster studies, and drafted and revised the manuscript. F.B. produced the fusion protein, performed thermal unfolding profiles, contributed to hamster studies, and drafted and reviewed the manuscript. C.D. contributed to BALB/c, K18-hACE2, and hamster studies and reviewed the manuscript. L.L. contributed to BALB/c studies and reviewed the manuscript. N.M. contributed to BALB/c studies. R.C. provided a crucial product and reviewed the manuscript. C.R. performed histological studies. M.M. produced viral strains. F.J. performed the neutralization test. L.M. performed clinical observations. M.C. F. provided in vitro human nasal mucosa. Y.Y. Monitored and controlled project development. A.B. Monitored and controlled project development. M. R. drafted and validated the ethical files for PFIE. A.T. provided the product. J.F.E. provided product. C.A.R. provided the product. F.H. performed a preliminary neutralization test. S.L. performed a preliminary protection hamster study. B.K. performed a preliminary protection hamster study. N.M. performed a preliminary protection hamster study. S.Z. performed a preliminary protection hamster study. S.P. supervised the neutralization analysis and reviewed the manuscript. M.N.M. contributed and supervised the BALB/c studies and reviewed the manuscript. N.A. designed the fusion protein, supervised the production, and drafted and reviewed the manuscript. M.E. contributed to project conception, designed hamster studies, performed the experiments, analyzed and interpreted the data, wrote the manuscript, and critically revised and edited the manuscript. I.D.P. conceived the project, acquired funding, supervised all the studies, and critically revised the manuscript. All authors read and approved the manuscript.

Competing interests
I.D.P., N.A., and M.E. are founders/equity holders in LovalTech. The remaining authors declare that the research was conducted without any commercial or financial relationships that could be construed as a potential conflict of interest.

Additional information
Supplementary information The online version contains supplementary material available at https://doi.org/10.1038/s41541-025-01123-y.

Correspondence and requests for materials should be addressed to Mathieu Epardaud or Isabelle Dimier-Poisson.

Reprints and permissions information is available at http://www.nature.com/reprints